Urban ventilation assessment with improved vertical wind profile in high-density cities – Comparisons between LiDAR and conventional methods

Yueyang He [a,b], Chao Yuan [c,*], Chao Ren [d], Edward Ng [a,b,e]

[a] *Institute of Future Cities, The Chinese University of Hong Kong, Hong Kong, China*
[b] *Institute of Environment, Energy and Sustainability, The Chinese University of Hong Kong, Hong Kong, China*
[c] *Department of Architecture, National University of Singapore, Singapore*
[d] *Division of Landscape Architecture, Faculty of Architecture, The University of Hong Kong, Hong Kong, China*
[e] *School of Architecture, The Chinese University of Hong Kong, Hong Kong, China*

ARTICLE INFO

ABSTRACT

The vertical wind speed profile is crucial to urban ventilation assessment and urban planning/design. This study uses Light Detection and Ranging (LiDAR) observation as benchmark to evaluate accuracy of wind profiles estimated by conventional methods. The conventional methods include Boundary Layer Wind Tunnel (BLWT), Regional Atmospheric Modeling System (RAMS), Power Law (PL), and Weather Research and Forecasting (WRF). The evaluation involves two typical urban sites with different densities under summer weak-wind conditions. Large Eddie Simulations (LES) are conducted to further investigate the sensitivity of urban ventilation assessment results to the deviations of wind profiles. The results indicate significant deviations in LES caused by conventional methods. The largest deviations of wind velocity ratio are found in mesoscale meteorological models (RAMS and WRF ($>$65%)). Deviations caused by physical and empirical models are smaller but still significant (BLWT ($>$25%) and PL ($>$40%)). Consequently, large deviations ($>$100%) of wind-relevant criterion for outdoor thermal comfort are observed. Finally, to balance accuracy and data availability, we recommend power law method as the optimal method to provide inflow boundary condition for numerical simulations when LiDAR observation is not available. We provide new and valuable understandings to improve urban ventilation assessment in high-density cities.

1. Introduction

Assessing urban ventilation plays an increasingly important role in supporting urban planning/design, especially for high-density cities suffering from weak wind conditions. The urban wind environment is crucial to inhabitants' comfort and health in terms of heat-stress relief (Blocken et al., 2009; Uehara et al., 2000; Yuan et al., 2020), as well as the pollutant and pathogen dispersion (Abbas and Dino, 2021; He et al., 2022b; Tominaga and Stathopoulos, 2018). It also contributes to buildings' energy saving by cooling roofs, facades, and other urban surfaces (Nikkho et al., 2017; Palyvos, 2008; Miguel et al., 2021). The assessment of microscale urban ventilation requires vertical wind speed profiles as essential boundary conditions in both physical (i.e. boundary layer wind tunnel (BLWT)) and numerical (i.e. computational fluid dynamics (CFD)) models. The wind profiles should be accurately

reproduced, since modeling results are sensitive to the initial conditions (Kent et al., 2018).

However, reproducing vertical wind speed profiles is challenging, mainly due to the practical difficulties in observing upper-air wind conditions especially over urban terrain (Barlow, 2014). Field measurements in the past relied on anemometers on balloons, tall towers, drones and even helicopters (Roth, 2000), but they are restricted by the duration, frequency, stability and height of the measurements. As alternatives to field measurements, empirical and modeling methods for estimating vertical wind speed profiles have been developed, which are reviewed in Section 2. However, these estimation methods are known to be ideal and more applicable to homogeneous terrain with adiabatic conditions, while roughness elements and land cover types in urban areas are heterogeneous. The vertical wind speed profiles are, therefore, highly variable due to the various sources and sinks of momentum and

---

heat (Gryning et al., 2011), and hard to be accurately estimated.

Characterized by high-density urban morphologies in the subtropics, Hong Kong suffers from weak wind conditions during hot and humid summer months. To better guide urban planning/design, the Planning Department, Hong Kong SAR Government established the Air Ventilation Assessment (AVA) system in 2006 (Ng, 2009). The AVA system is designed for meeting the needs of sustainable urban planning/design practices by identifying and minimizing the potential negative impact of new development projects on the urban wind environment in Hong Kong. It has been implemented in Hong Kong local planning exercises for over 15 years. Meanwhile, its methodology has also been adopted by other high-density cities, such as Macau (Tieben et al., 2015), cities in mainland China (Ren et al., 2018), Singapore (National University of Singapore, 2021), and Brisbane (Australian Institute of Architects, 2021). AVA provides a systematic methodology to assess pedestrian-level wind environment using either wind tunnel or CFD, and requires all major developments in Hong Kong to optimize their designs (Housing, Planning and Lands Bureau (HPLB) and Environment, Transport and Works Bureau (ETWB), 2006). The Planning Department (PlanD, 2013a) subsequently published a vertical wind profile dataset, named "site wind availability data", of 13 typical sites by wind tunnel experiments, and later extended it to the city's whole territory by mesoscale meteorological modeling. This dataset aims to provide boundary conditions of inlet wind profiles to AVA tests at different urban areas.

However, despite all the achievements, the AVA system still needs to be critically reviewed and updated due to the two main limitations of the existing site wind availability data. Firstly, this dataset was developed by the wind tunnel and mesoscale meteorological modeling, and has never been validated by field observation. Secondly, the dataset does not take into account the "new normal" wind condition in summer with increasingly frequent and intense extreme hot weather events caused by global climate change as reported by the Hong Kong Observatory (HKO, 2021a). To address the above two limitations, there is a need to conduct long-term field observation on vertical wind speed profiles in high-density areas in Hong Kong especially during summer.

The recent development of ground-based remote sensing technologies, which are reviewed in Section 2, such as wind Light Detection and Ranging (LiDAR), provides a new and reliable alternative to measure vertical wind speed profiles on sites. Hence, focusing on wind LiDAR observation and data analysis, we conduct two studies to address two above-mentioned limitations of the site wind availability data separately. The first study (the current paper) aims to address the first limitation, i.e., lack of validation, by evaluating the accuracy of wind profiles estimated by conventional methods and the sensitivity of CFD-based urban ventilation assessment results to the deviations of these wind profiles. Specifically, the conventional methods involved are the BLWT method (PlanD, 2010), the Regional Atmospheric Modeling System (RAMS) method (PlanD, 2013b), the Power Law (PL) method (HPLB and ETWB, 2006), and the Weather Research and Forecasting Model (WRF) method (Institute for the Environment (IENV), 2021). Compared with the first study, in which CFD simulations are conducted in neutral thermal conditions (i.e. heat transfer is ignored), the second study (another paper (He et al., 2022a)) aims to address the second limitation, i.e., lack of consideration on extreme heat in summer, by including buoyancy effects in both the measurement and modeling work.

Section 2 reviews the previous studies of vertical urban wind profiles. Section 3 uses the LiDAR and conventional methods to reproduce the vertical wind speed profiles, which are adopted as CFD inputs. In Section 4, the CFD models for urban ventilation simulations are set up and validated. Section 5 cross-compares the CFD results with different input wind profiles, as well as quantifies the deviations of different conventional methods from the LiDAR method. Finally, the conclusion and limitation are given in Sections 6 and 7, respectively.

2. Literature review

2.1. Conventional studies on vertical urban wind profiles

At high-density urban areas, vertical wind speed profiles are highly modified by surface roughness due to the large frictional drag, and continuous efforts have been made to predict them accurately (Barlow, 2014). Based on sparse available field observational data, early research described urban wind speed profiles under spatially-averaged and temporally-averaged effects of turbulent motions (Taylor, 1915). As illustrated in Fig. 1, Oke (2004) generalized the structure of an urban mean wind speed profile under neutral stratification, where the wind speed decreases gradually with heights above the urban canopy layer while it becomes almost constant with heights below the displacement height until quite close to the ground surface. Empirical formulas have been used to further quantify the characteristics of the urban wind speed profiles. Among them, the power law and log law are most widely used. For representing the surface roughness of urban terrain, a typical power law index is suggested to be 0.21–0.5 (Architectural Institute of Japan (AIJ), 1996; Davenport, 1967; Irwin, 1967; Rossby and Montgomery, 1935), while a typical range of roughness length in the log law is 1–4 m (Engineering Sciences Data Unit, 1985; Lettau, 1969; Sutton, 1947; Wieringa, 1992). Meanwhile, some other empirical formulas were proposed, such as the Deaves and Harris model (Deaves and Harris, 1978), and Gryning model (Gryning et al., 2007), but they are more difficult in mathematical manipulation. A well-known deficiency of most of the existing empirical models is that they are only applicable to homogeneous and adiabatic boundary layers rather than heterogeneous and convective ones (Kent et al., 2018). Furthermore, most existing empirical models assume surface roughness parameters as a constant, while they could be variable in reality (Lim et al., 2017).

Recent advances in computational power have made mesoscale meteorological modeling, such as MM5, RAMS and WRF, increasingly popular to predict boundary layer flow over cities (Pielke Sr, 2013). Mesoscale meteorological models adopt different planetary boundary layer schemes and urban canopy schemes to parameterize the subgrid-scale turbulent mixing of momentum, heat and moisture in the atmosphere, as well as their interactions with urban surfaces. The accuracy of mesoscale meteorological models is sensitive to the performance of numerical schemes (Stull, 1988). For example, Hu et al. (2010) and Xie et al. (2012) evaluated several local and non-local boundary layer schemes in WRF, and found that the non-local schemes better treat the thermally-induced vertical mixing in convective conditions, and
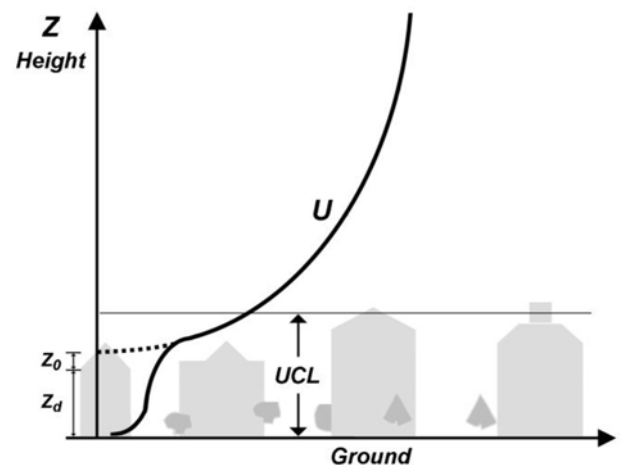

Fig. 1. Diagram of a generalized mean wind speed profile at a high-density urban site within urban canopy layer (*UCL*), where Z_0 is roughness length and Z_d is zero-plane displacement length (note: this figure was modified according to Oke (Oke, 2004)).

have less bias with field observation. Steeneveld et al. (2011) compared several boundary layer schemes in RAMS and WRF, and indicated the inconsistent performance of these schemes in two meteorological models. Besides, Wong et al. (2019) found an obvious improvement of the predicted urban wind speed and temperature in WRF by a multilayer urban canopy scheme (Salamanca et al., 2011) compared with a bulk urban canopy scheme. They further suggested that the modeling results were more sensitive to the urban canopy schemes than the boundary layer schemes. However, the current computational power still restricts the horizontal grid resolution to be finer than several hundred meters (Martilli, 2007), which is required by urban canopy schemes. This means that the real urban heterogeneities cannot be explicitly resolved, which affect the modeling accuracies of near-ground attributes.

2.2. Recent LiDAR studies of vertical urban wind profiles

As a new alternative, wind LiDAR has been increasingly used to investigate boundary layer flow over cities, as well as to observe and quantify the vertical urban wind speed profiles (Barlow et al., 2011; Lane et al., 2013; Park and Chae, 2018). For example, Drew et al. (2013) observed the hourly-averaged wind speed profile in central London and compared it with several empirical models. They found that the empirical models overestimated the wind speed, particularly during a strong wind period, due to the lack of detailed representation of urban heterogeneities. After that, Kent et al. (2018) further extrapolated and evaluated more empirical models based on a LiDAR observation in central London during a strong wind period. Their results indicated consistent underestimations of wind speed by empirical models when the height variability was not involved in the surface roughness parameters. Kikumoto et al. (2017) observed the hourly-averaged wind speed profile in Tokyo and evaluated the accuracy of the power law formula. They suggested that the power law formula could be applicable during a strong wind period, while its accuracy decreased with low wind speed and short average time intervals. Later, Lim et al. (2017) further identified the significant variations of the power law index during different time periods based on a LiDAR observation in Tokyo. Sepe et al. (2018) observed the 10-min-averaged wind speed profile in Napoli, and calibrated the surface roughness parameters used in the log law and other formulas. Meanwhile, studies have also been conducted to detect the urban boundary layer heights, such as in London (Kotthaus et al., 2018), Paris (Menut et al., 1999), Houston (Haman et al., 2012), and Beijing (Huang et al., 2017).

More recently, the LiDAR method has been introduced to investigate the boundary layer flow in Hong Kong. Yim (2020) identified the mean wind speed profiles during four seasons as well as in hot-and-polluted episodes regardless of the variations of wind directions. Their results provided insights on the transboundary pollutant dispersion in the city. Later, based on three wind LiDAR, He et al. (2021) observed the evoluations of hourly-averaged wind speed profiles at the upwind, downtown and downwind locations in Hong Kong under a summer prevailing wind direction. They quantitatively described the boundary layer heights and wind profile shapes at respective sites. Despite these research outcomes, there is a lack of study on how well the LiDAR method can improve the accuracy of CFD simulation results of pedestrian ventilation, and what are the deviations caused by inflow boundary conditions reproduced by conventional methods. A critical study of their accuracy is indispensable, given that the simulation results can significantly affect the decision making in urban planning/design, especially in high-density cities with weak wind conditions.

3. Reproduction of vertical urban wind profiles at test sites

In this section, we reproduced vertical urban wind profiles at the test sites of Hong Kong, by the LiDAR and above-mentioned conventional methods, i.e., BLWT, RAMS, PL, and WRF. The wind profiles are adopted as the inflow boundary conditions of CFD simulations as described in

Section 4. Total two typical urban sites are selected in 1) Sai Wan and 2) Sai Kung, as shown in Fig. 2. The selected urban sites have different surface morphological features: Sai Wan is a fully-developed downtown district of northwestern Hong Kong Island, with high-rise buildings and hilly surrounding topography; and Sai Kung is a new town district of southeastern New Territories, with sparse urban and rural developments. The building features of the source areas (e.g., yellow cells in Fig. 2) are quantified in Fig. 3. Overall, the source area in Sai Wan has a ground coverage ratio of over 40% with a mean building height of over 40 m, while the source area in Sai Kung halves the ground coverage ratio to around 18% with most of the buildings below ten stories. According to the recommendations by AIJ (1996), the two source areas can be categorized as a city center and a city, respectively.

3.1. Light Detection and Ranging (LiDAR) method

The LiDAR method is based on the field observation of the ground-based and long-range wind LiDAR (model: WindCube 100S). In the fields, the wind LiDAR emitted laser beams to the atmosphere and then captured those backscattered by the aerosols. The wind-induced aerosol particle movements caused Doppler shifts (Δf) (i.e., changes in frequency of the laser beams), which is calculated by the following equation:

$$\Delta f = f - f_0 \tag{1}$$

where f_0 and f refer to the frequency of the emitted and backscattered laser beams, respectively. The detected Δf was then used to calculate the vertical wind speed profiles based on the Doppler Beam Swinging (DBS) scan mode. Each scan cycle took approximately 20s, ranging from 50 m to up to 3 km above the scanner at a range gate (i.e., discrete interval) of 25 m. More details of the DBS scan mode and the calculation of wind profiles are attached in Appendix A. An on-site validation study of the wind LiDAR is attached in Appendix B.

We used two wind LiDAR to simultaneously observe the wind profiles over two selected sites (Fig. 2). The observation was conducted in the summer period from 1 June to 31 August 2020, to tackle the wind that is most needed for heat-stress relief (Ng, 2009). In the temporal dimension, we focused on the prevailing southwest wind conditions. We, therefore, excluded the data from other wind directions (i.e., $\theta < 180°$ or $\theta > 270°$), as well as those in the periods with a typhoon or low data availability. The remaining wind data was then used to reproduce hourly-averaged wind profiles. In the spatial dimension, the lowest data points were 65 m and 50 m above the ground at the sites in Sai Wan and Sai Kung, respectively. They were determined by the location heights of LiDAR, as well as their blank scanning distance of 50 m above the scanner.

A cross-comparison of the two LiDAR wind speed profiles over Sai Wan and Sai Kung is shown in Fig. 4. Significant impacts of the high-density urban sites on the boundary layer wind conditions are confirmed. The result suggests much larger vertical wind speed gradients over a city center (Sai Wan) than a city (Sai Kung). Particularly, it suggests a distinct difference of wind speed of 1.8 m/s over the surfaces of two categories of high-density urban terrain in Hong Kong. These two LiDAR wind profiles are used as a benchmark to evaluate other wind profiles developed by the conventional methods in Figs. 5 and 6.

3.2. Conventional methods

To be cross-compared and evaluated by the results from LiDAR, conventional methods, which were reviewed in Section 2, i.e., BLWT method, RAMS method, WRF method, and PL (Power Law) method, were used to develop vertical wind speed profiles in this study. Amongst them, BLWT, RAMS, and PL use the site wind availability data published by the Planning Department. WRF has been increasingly used recently due to its capability to predict real-time meteorological conditions in

Fig. 2. Two selected high-density urban sites (800 m × 800 m) in Hong Kong for reproducing vertical wind speed profiles, and the locations of nearby ground-based wind LiDAR, as well as the corresponding source points/cells for estimating vertical wind speed profiles by conventional methods (i.e., BLWT, RAMS, and WRF).
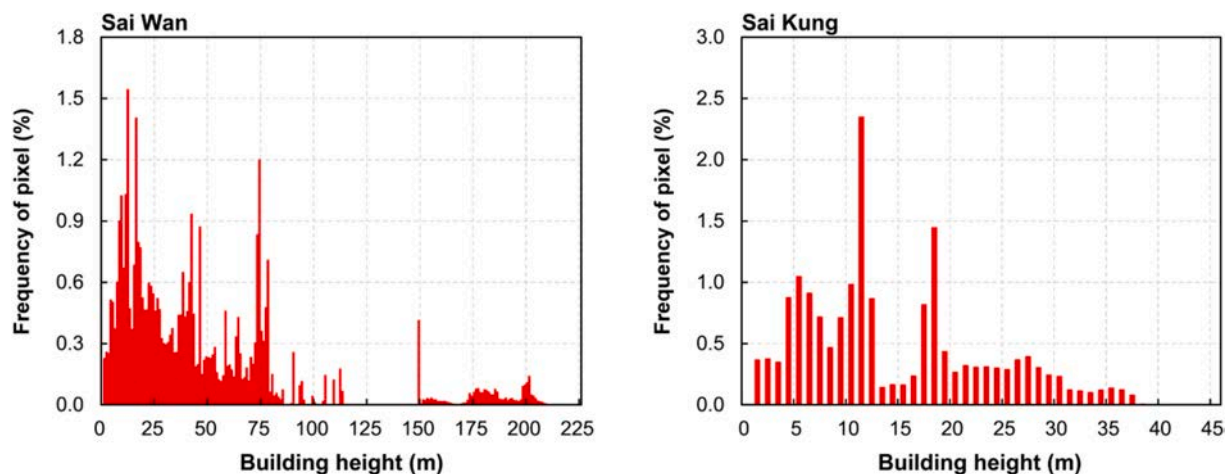

Fig. 3. Frequency of pixel of different building heights at two source areas (i.e., yellow cells in Fig. 2) of two ground-based wind LiDAR. (For interpretation of the references to colour in this figure legend, the reader is referred to the Web version of this article.)

Hong Kong. The key technical parameters of these methods together with the LiDAR method are shown in Table 1, and cross-compared further in this section. To have a fair evaluation, the temporal and spatial conditions were kept as similar as possible in the LiDAR and conventional methods when reproducing the wind profiles.

3.2.1. Boundary layer wind tunnel (BLWT) method

A vertical wind profile dataset, i.e., site wind availability data, was developed using the BLWT method and published by the Planning Department (PlanD, 2013a). This dataset was established for 13 typical sites in Hong Kong with 16 cardinal wind directions, via low-speed and adiabatic wind tunnel experiments from 2006 to 2009. The experiments reproduced the characteristics of non-typhoon wind approaching Hong Kong at the inlet in accordance with the long-term wind speed measured by the automatic weather station at an upwind site of Hong Kong (i.e., Waglan Island (HKO, 2021b)) and the shapes of mean wind speed and turbulence intensity profiles over open sea surface stipulated in the Australian/New Zealand Standard (AS/NZS 1170.2:2002 (Zealand,

2002)). This inlet profile was then developed through a long tunnel section with 1: 2000 reduced-scale realistic topography and building models surrounding the target sites. At the end, the vertical wind speed profiles over the respective sites were measured by miniature dynamic pressure probes at 9 heights. Meanwhile, all buildings within a radius of 500 m of the sites were removed to eliminate the impacts from the immediate surroundings (PlanD, 2010). A diagram and more details of the wind tunnel facility is attached in Appendix C.

In this study, we used the data from BLWT sites, which are nearest to two LiDAR sites, as shown in Fig. 2. To be compared with the LiDAR wind profiles, the BLWT wind profiles at sites were developed by averaging 5 wind profiles from the southwest wind directions (i.e., $180° \le \theta \le 270°$). The hourly-averaged wind speed measured at Waglan Island during the study period (i.e., summer 2020) was used as a reference to correct the inlet wind speed at the same height in the wind tunnel experiments, so as to be consistent with the previous experimental setup following the AVA technical circular (HPLB and ETWB, 2006). The BLWT wind profiles are plotted in Figs. 5 and 6.
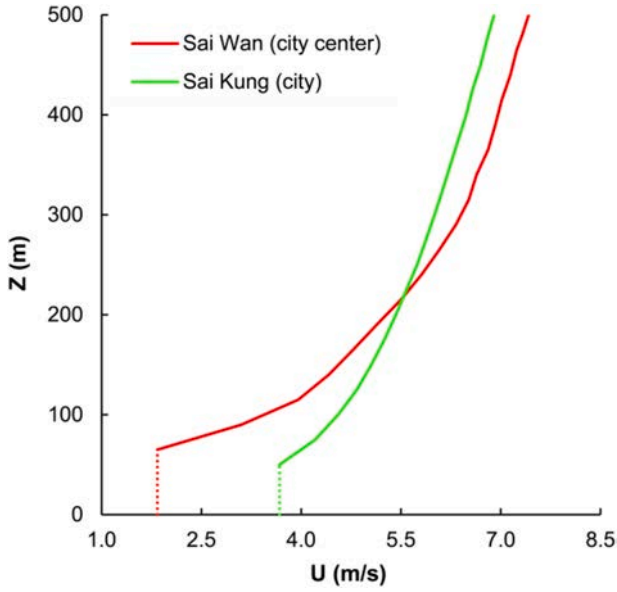
Fig. 4. Vertical wind speed (*U*) profiles observed by wind LiDAR under prevailing southwest wind direction over Sai Wan and Sai Kung in summer 2020.

3.2.2. Regional Atmospheric Modeling System (RAMS) method

Different from BLWT, in which the site wind availability data is from wind tunnel experiments, this RAMS dataset was developed by RAMS modeling (version 6.0) in a period of 10 years from 2000 to 2009, which was also published by the Planning Department (PlanD, 2013b) as site wind availability data. The RAMS modeling contained three nested domains, where the innermost domain covered the whole territory of Hong Kong in a horizontal resolution of 0.5 km × 0.5 km and vertical resolutions stretching from 25 m near ground level till over 500 m at upper levels. In each computational cell, the annually-averaged vertical wind speed profiles are provided, as shown in Table 1. Seasonally, however, RAMS only provide averaged reference wind speed at a domain height (i.e., 500 m), and no vertical wind speed profiles are provided in summer. The RAMS modeling input the reanalysis data from the US National Centers for Environmental Prediction (NCEP) in a spatial resolution of 0.5° (latitude) × 0.5° (longitude) and a temporal resolution of 6 h. The modeling was nudged with the near-ground wind

and temperature data from local automatic weather stations (HKO, 2021b). Meanwhile, the effects of urban heterogeneities were represented by the algorithms of realistic topographical heights and the different classes of surface land uses.

In this study, we directly adopted the annually-averaged vertical wind speed profiles from the cells, which cover two LiDAR sites, as shown in Fig. 2. The southwest wind direction sector (i.e., $202.5° \leq \theta \leq 292.4°$) were selected for cross-comparison. The RAMS wind profiles are plotted in Figs. 5 and 6.

3.2.3. Power law (PL) method

The PL method in this paper was defined as a hybrid method integrating the RAMS dataset with the power law empirical formula. This method downscales the meteorological modeling results from mesoscale to microscale by using the RAMS dataset to calculate the reference wind speed at 500 m's height and the power law to estimate the shape of the vertical wind profile according to the AVA technical circular (HPLB and ETWB, 2006). Different from the annually-averaged RAMS profiles, the PL profiles are summer-averaged vertical wind speed profiles as summer-averaged RAMS data is available at 500 m's height. In this study, the summer-averaged vertical wind speed profiles were extrapolated as:

$$U = U_\infty \left(\frac{Z}{Z_\infty} \right)^a \qquad (2)$$

where *U* denotes the wind speed at different heights (*Z*); U_∞ denotes the summer-averaged wind speed simulated by RAMS at the height of 500 m (Z_∞) in the cells covering the two LiDAR sites (Fig. 2), from the southwest wind direction sector (i.e., $202.5° \leq \theta \leq 292.4°$); and *α* is the power law index related to terrain roughness. As described in Fig. 3, the terrain of the two sites covered by the RAMS cells in Sai Wan and Sai Kung can be categorized into a city center and a city (AIJ, 1996), respectively. Hence, to appropriately represent the terrain roughness, this study referred to a widely-used classification (AIJ, 1996) and assigned *α* = 0.35 and 0.27 to the two sites, respectively. The PL wind profiles are plotted in Figs. 5 and 6.

3.2.4. Weather Research and Forecasting Model (WRF) method

The WRF method is based on the real-time hourly-simulated wind data provided by the Institute for the Environment, the Hong Kong University of Science and Technology (IENV, 2021). The dataset is developed by WRF modeling (version 4.3), where four nested domains
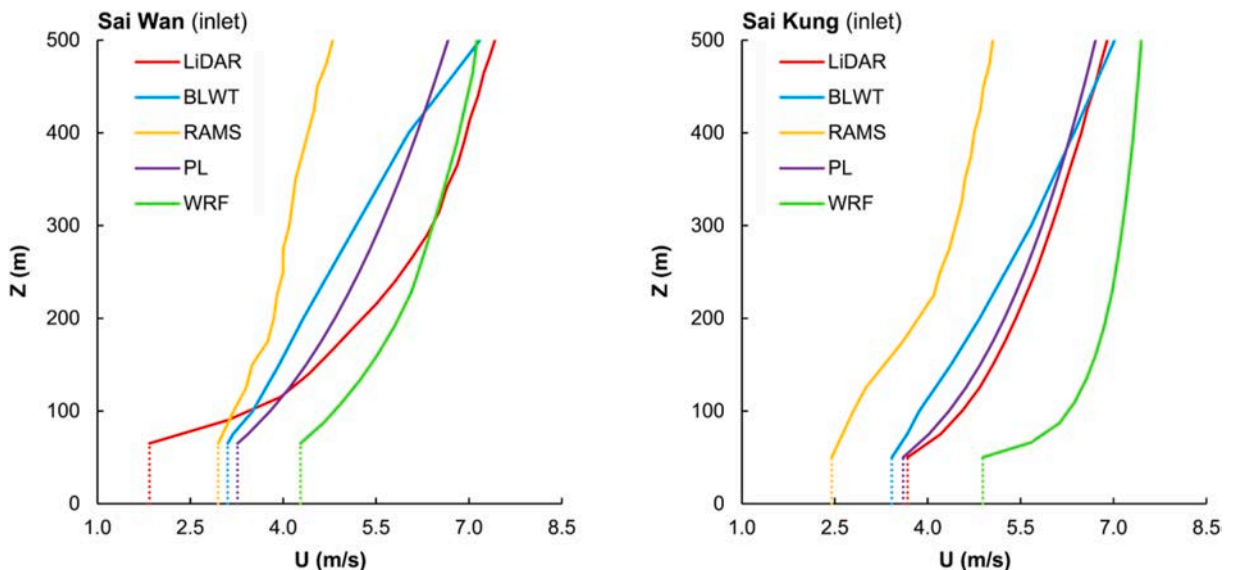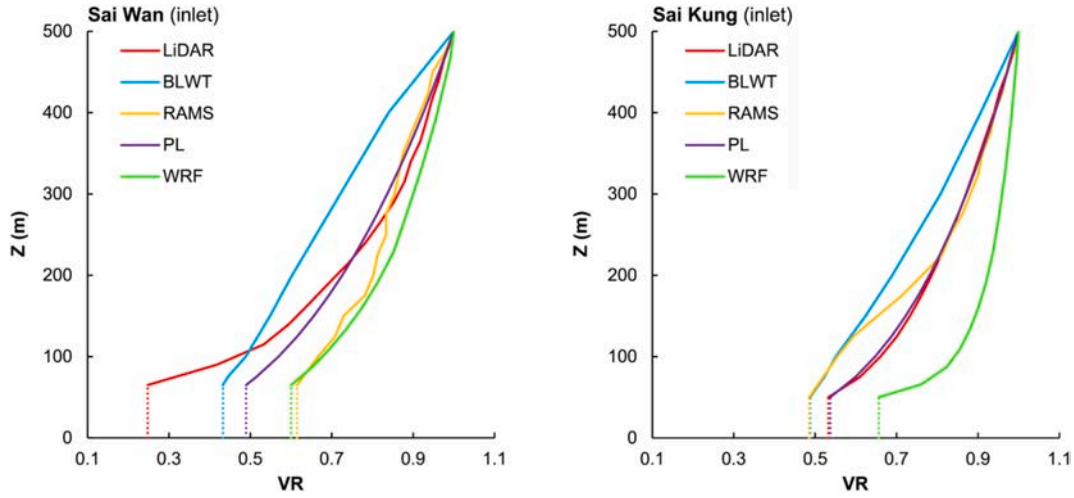

Fig. 5. Vertical wind speed (*U*) profiles developed by the LiDAR and conventional methods (BLWT, RAMS, PL and WRF) in Sai Wan and Sai Kung.

Fig. 6. Vertical wind velocity ratio profiles ($VR = U/U_\infty$, where U_∞ is the wind speed at the height of 500 m of the respective method), developed by the LiDAR and conventional methods (BLWT, RAMS, PL and WRF) in Sai Wan and Sai Kung.

Table 1
Parameters in LiDAR and conventional methods to estimate vertical wind speed profiles as inputs for CFD simulations (note: wind direction division refers to the number of wind directions divided in 360°).

Method	Highest data point (m)	Lowest data point (m)	Wind direction division	Temporal resolution	Model type
LiDAR	3000	65/50	360	Hourly	Observed
BLTW	500	25	16	N.A.	Physical
RAMS	500	12.5	4	Annual	Numerical
PL	500	0	16	Seasonal	Empirical
WRF	2700	25	360	Hourly	Numerical

were applied. The innermost domain, which covered the Hong Kong territory, adopted a horizontal grid resolution of 1 km × 1 km, and vertical resolutions stretching from around 18 m near ground level till around 400 m at upper levels. The modeling was initialized by the NCEP data in a spatial resolution of 1° (latitude) × 1° (longitude) and a temporal resolution of 6 h. Near-ground wind data in Hong Kong was used for observation nudging at the surface of the innermost domain (Xie et al., 2012). To parameterize atmospheric and urban surface conditions, the modeling applied a local boundary layer scheme, and a multilayer urban canopy scheme coupling the building effect parameterization and the building energy model (Salamanca et al., 2010).

To obtain the vertical wind speed profiles by the WRF method, we used the data from the WRF cells covering the two LiDAR sites as shown in Fig. 2. In each cell, the wind profiles were obtained by extracting and averaging the hourly-simulated wind profiles from the southwest wind direction (i.e., $180° \leq \theta \leq 270°$) during the study period (i.e., summer 2020). The WRF wind profiles are plotted in Figs. 5 and 6.

3.3. Cross-comparison of vertical urban wind profiles

The vertical wind speed profiles obtained by the LiDAR and conventional methods (BLWT, RAMS, PL and WRF) are plotted together in Fig. 5 for cross-comparison. The LiDAR profiles, as the observation results, were used as a benchmark to evaluate conventional methods and to identify the optimal one. To indicate how much of the wind availability of a site could be experienced at different heights, the vertical wind speed profiles are converted into the vertical wind velocity ratio (VR) profiles in Fig. 6, following the AVA technical circular:

$$VR = \frac{U}{U_\infty} \tag{3}$$

where U and U_∞ refer to the wind speed at an evaluation height and the height of 500 m, respectively.

As shown in Fig. 6, overall, the conventional methods reveal significant deviations of the near-ground VR from the LiDAR method. Among the conventional methods, larger deviations are seen in the mesoscale meteorological modeling methods (RAMS and WRF), and smaller deviations are in the methods based on physical and empirical models (BLWT and PL). Furthermore, the conventional methods indicate smaller deviations of the near-ground VR in Sai Kung than Sai Wan. This implies that the conventional methods more accurately predict the shapes of wind profiles in Sai Kung. However, it should be noted that the vertical VR profiles cannot explain the deviations of U_∞, which are found to be significant at both sites, especially for RAMS (Fig. 5). The largest deviations of RAMS are due to its too low temporal resolution (Table 1), to specify the wind availability during summer periods.

4. CFD simulations

More than comparing the wind profiles themselves, we conducted CFD simulations using wind profiles from Section 3 to investigate the assessment deviation, which could be caused by the deviations of these wind profiles. CFD simulations have been widely adopted to predict wind conditions in urban settings (He et al., 2018, 2019), using either Reynolds-averaged Navier-Stokes (RANS) or large eddy simulation (LES) turbulence models. In this study, Parallelized LES Model (PALM) version 6.0, based on the filtered and incompressible Navier-Stokes equations, was applied in CFD simulations. Compared with RANS models, the LES model is more accurate, as it explicitly resolves the instantaneous large eddies in resolved-scales and only parameterizes the closures of the small eddies in subgrid-scales (Maronga et al., 2020). As a bulk part of energy is contained in the large eddies, up to 90% (Heus et al., 2010) of the turbulence energy can be resolved by the LES model. PALM has been validated in high-density urban settings, such as by Resler et al. (2021), Gronemeier et al. (2020), and Wang et al. (2020). To further validate PALM, this paper conducted two validation studies as attached in Appendix D.

4.1. Settings of computational geometry, domain and grids

Two urban sites in a size of 800 m (X) × 800 m (Y) near two wind LiDAR in Sai Wan and Sai Kung, as shown in Fig. 2, were selected for CFD simulations. These two selected simulation sites have relatively flat terrain, and therefore only building geometries were involved in the LES model. To reproduce the building geometries, building height

information was input from the geographic information system in a raster data format (i.e., ASCII format (PALM group, 2022)) with the same resolution as the horizontal computational grids. In this sense, each grid cell is either 100% fluid or 100% obstacle. We set the size of the computational domain as 2800 m (*X*) × 800 m (*Y*) × 500 m (*Z*), referring to the recommendations by AIJ guidelines (Tominaga et al., 2008) and previous PALM studies (Wang et al., 2020; Wang and Ng, 2018). As shown in Fig. 7, in the streamwise direction (i.e., *X* direction), the domain leaves a buffer distance at the windward side of the urban model which compromises the impacts of building blockages and wall-function roughness modifications (Blocken et al., 2007) on the inlet wind profiles. A sensitivity test was conducted in an empty domain to identify the horizontal inhomogeneity phenomenon of an inlet wind profile as attached in Appendix E. A buffer distance is also set at the leeward side of the urban model to allow the outflow to be freely developed before it reaches the outlet. In the spanwise direction (i.e., *Y* direction), to reduce the computational cost, we set no buffer distance at the lateral sides of the urban model, and assume that the urban area is continuous and extended outward from the domain. This assumption adopted a high blockage ratio (i.e., around 15%) and cyclic conditions were applied to minimize the artificial impacts caused by the domain lateral boundaries.

PALM is based on cartesian computational grids, where the cell size is constant in the horizontal dimensions. To determine the proper cell sizes in PALM for a high-density urban model, a grid-sensitivity test has been conducted by Gronemeier et al. (2017) to compare the cell sizes of 1 m, 2 m, 4 m and 8 m, in terms of the near-ground wind speed in Kowloon City, Hong Kong. Their result indicated a diminishing change of the wind fields with the cell sizes reduced from 8 m to 2 m, where the difference between the cell sizes of 1 m and 2 m was marginal. Meanwhile, however, the increment of the simulation time is sharply increasing. As a compromise between the simulation accuracy and computational cost, this paper adopted the cell size of 2 m in the horizontal dimensions. In the vertical dimension, a smaller cell size of 1 m was adopted from the ground surface to the height of 25 m to more explicitly simulate the near-ground flow, and a slight stretching ratio of 1.03 was applied to the cells at the upper levels. In this way, the total cell number was counted to be 1400 (*X*) × 400 (*Y*) × 120 (*Z*). Fig. 8 shows the computational grid generated for an urban model.

4.2. Settings of boundary conditions, numerics and runtime

The flow to be solved was neutrally stratified in the simulations. At the inlet, the vertical wind speed profiles obtained in Section 3 were prescribed to develop the turbulent inflow boundary conditions. To exclude the impacts of the missing data (Table 1) in different methods, all prescribed vertical wind speed profiles were within the same ranges between the highest data points of 500 m, and the lowest data points of 65 m and 50 m at the sites of Sai Wan and Sai Kung, respectively. From the heights of the lowest data points till the ground surfaces, the inlet wind speed was assumed to be constant in respective methods. In this sense, a fair comparison was conducted between the LiDAR and the conventional methods, in terms of the site wind availability at the same heights at respective sites. This assumption is close to the reality in high-density urban areas, as described in Fig. 1 according to Oke (2004), and Bentham and Britter (2003), where the wind speed gradient inside urban canopies is usually small below the displacement height until quite close to the ground surface.

The turbulent inflow boundary conditions were generated by the synthetic turbulence method according to Xie and Castro (2008), which imposed spatially and temporally correlated perturbations each time step onto the velocity components. At each time step (*t*), the instantaneous wind speed component (u_i) at the inlet was calculated by the following equation:

$$u_i(t) = \overline{u}_i(t) + \alpha_{ij}(t) u_j'(t) \tag{4}$$

where $i, j \in \{1, 2, 3\}$; $\overline{u}_i$ refers to a mean wind speed component; α_{ij} refers to an amplitude tensor derived from the Reynolds stress tensors. Due to the lack of measurement data, PALM assumed that the Reynolds stress tensor depended on the heights above the ground and parametrized its components by the equations according to Rotach et al. (1996) with the friction velocity estimated from the mean horizontal wind speed at the first vertical grid point; and u_j' refers to a turbulent motion, which was obtained by the following equation:

$$u_j'(t) = u_j'(t - \Delta t) exp\left(\frac{-\pi \Delta t}{2T}\right) + \psi_j(t - \Delta t)\left[1 - exp\left(\frac{-\pi \Delta t}{T}\right)\right]^{0.5} \tag{5}$$

where ψ_j refers to a set of random data generated independently in PALM at each time step, with a zero mean and a unity variance; Δt refers to the interval of 1 time step; and *T* refers to the Lagrangian time scale, which was assumed to be a constant input for the whole inlet and calculated automatically from computed data (Xie and Castro, 2008). The resolved-scale momentum flux profiles were confirmed to be much larger (i.e., at least one magnitude larger) than the subgrid-scale momentum flux profiles for activating the energy-containing eddies.
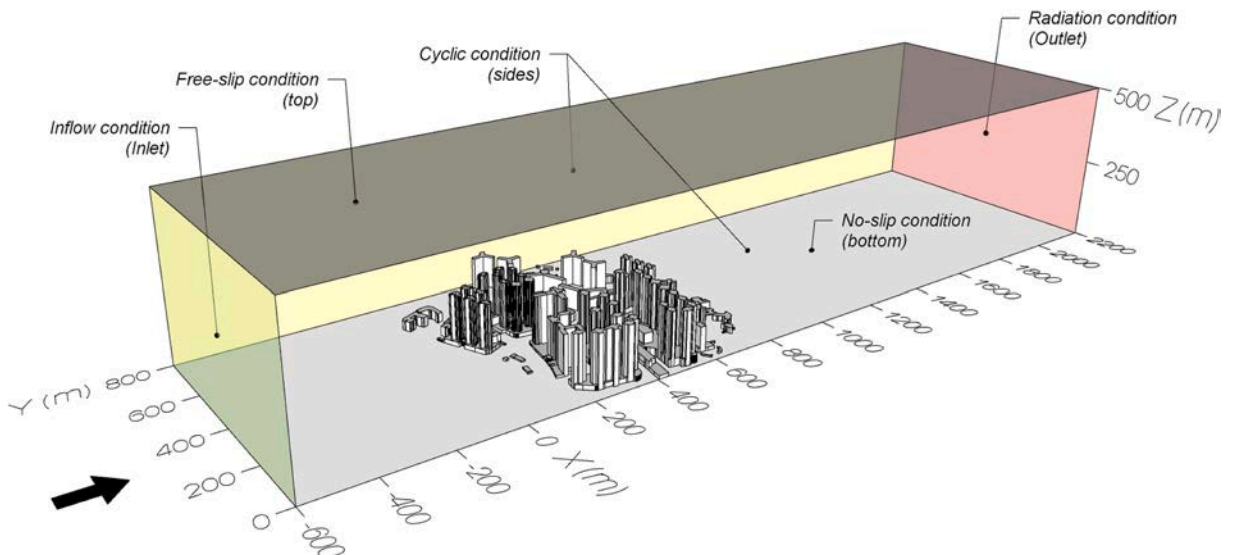

Fig. 7. Computational domain and boundary conditions in the LES with an urban model.
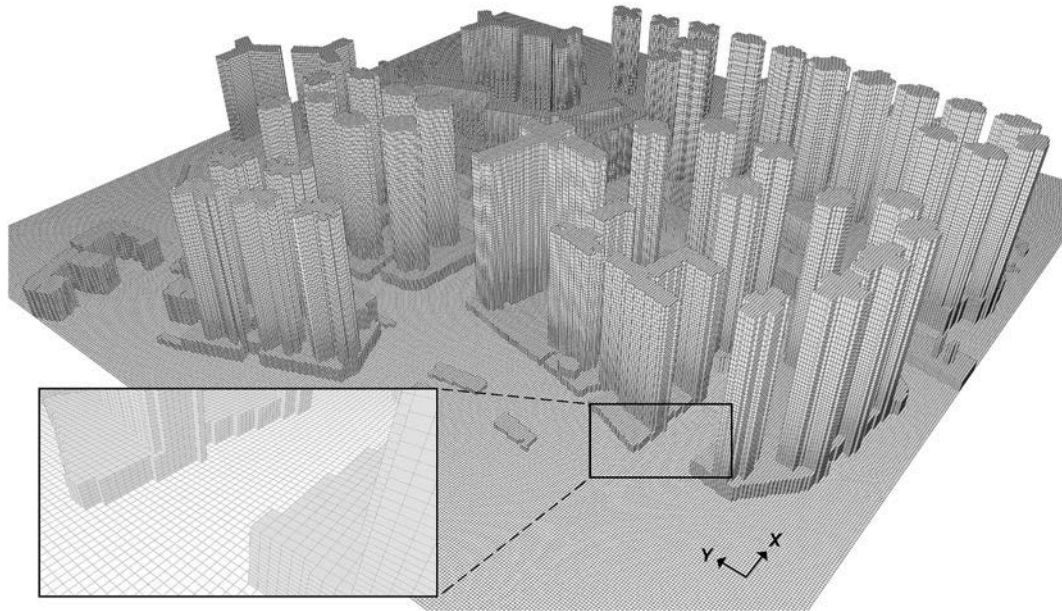
Fig. 8. Computational grid in the LES for an urban model with an enlarged view of cells near the ground and podiums.

Besides the inlet, no-slip and free-slip conditions were applied to the domain bottom and top boundaries, respectively. A radiation condition was used at the outlet to allow the eddies to freely leave the domain. Additionally, the settings of numerics and runtime in the LES model are summarized in Table 2.

5. Results and discussion

In this section, we cross-compare the CFD results using wind profiles from Section 3. Firstly, Section 5.1 provides qualitative analysis results of the pedestrian-level *VR* assessment. Furthermore, Sections 5.2 and 5.3 provide quantitative analysis to reveal the deviation results of different conventional methods from the LiDAR method at the pedestrian and upper levels, respectively. In Section 5.4, an overall evaluation is given to different conventional methods for identifying the optimal one.

5.1. Contours of wind velocity ratio at the pedestrian level

The distributions of *VR*, which were simulated by CFD with different wind profiles, are shown in Figs. 9 and 10. The CFD simulation results based on LiDAR wind profiles were adopted as a benchmark. In line with the cross-comparison among inlet *VR* profiles themselves (Fig. 6), all conventional methods (BLWT, RAMS, PL and WRF) cause significant deviations on the pedestrian-level *VR* assessment. Overall, the results suggest larger deviations on the mesoscale meteorological modeling methods (RAMS and WRF) than the physical and empirical modeling

Table 2
Simulation settings of numerics and runtime.

PALM parameter	Setting and description
Pressure solver	Multigrid scheme
Advection scheme	Fifth-order upwind scheme
Turbulence closure	1.5-order closure
Temporal discretization	Third-order low-storage Runge–Kutta scheme
Total simulation time	5400 s
Output simulation time	The last 1800 s (where simulation result was averaged and outputted)
Courant number	< 1
Mean time step interval	< 1 s

methods (BLWT and PL). These deviations are obviously bigger in Sai Wan than in Sai Kung. The different results in Sai Wan and Sai Kung suggest that the reliability of the conventional methods can vary substantially according to the surface morphologies and surrounding topography of the site.

In Sai Wan, as shown in Fig. 9, all conventional methods significantly overestimate *VR*, compared with the LiDAR method. Overall, the largest overestimations are observed at the upwind side of the target area, while they become smaller at the target area as the inflow is modified by the urban surface roughness. Specifically, amongst different conventional methods, the RAMS and WRF methods lead to the most obvious overestimations in respect of the LiDAR method. This result is consistent with the near-ground observation conducted by Wong et al. (2019). There are two main reasons for the deviations. Firstly, the current mesoscale meteorological models tend to underestimate the surface roughness in high-density urban areas due to the coarse computational grid, and therefore underestimate the wind speed gradients in reality. Secondly, the model accuracy is also affected by the parametrization of the subgrid-scale turbulent motions, which simplifies the coupling effects of the momentum, heat and moisture in the atmosphere (Martilli, 2007). More importantly, the deviation caused by the BLWT and PL methods are less significant than the RAMS and WRF methods, even though overestimations were still observed. For the BLWT method, the main reason for the deviations is probably that the physical model removes the buildings within a radius of 500 m when measuring the wind profiles in the wind tunnel, as mentioned in Section 3.2.1, and hence overestimates the near-ground *VR* due to the underestimated surface roughness. For the PL method, similar overestimations of the near-ground *VR* have been reported by Drew et al. (2013). They attributed these deviations to idealizing the nature of realistic urban surfaces. In addition, the deviations may be also attributed to the known deficiency of the power law formula on describing the lower boundary layer flow as indicated by Counihan (1975).

The difference between the LiDAR and conventional methods in Sai Kung with lower density is less significant than the urban area with higher density, i.e., Sai Wan. As shown in Fig. 10, in respect of the LiDAR method, a significant difference is only observed at the BLWT and WRF methods, by which the pedestrian-level *VR* are either underestimated or overestimated, respectively. The two remaining conventional methods (RAMS and PL) are in close agreement with the LiDAR method.
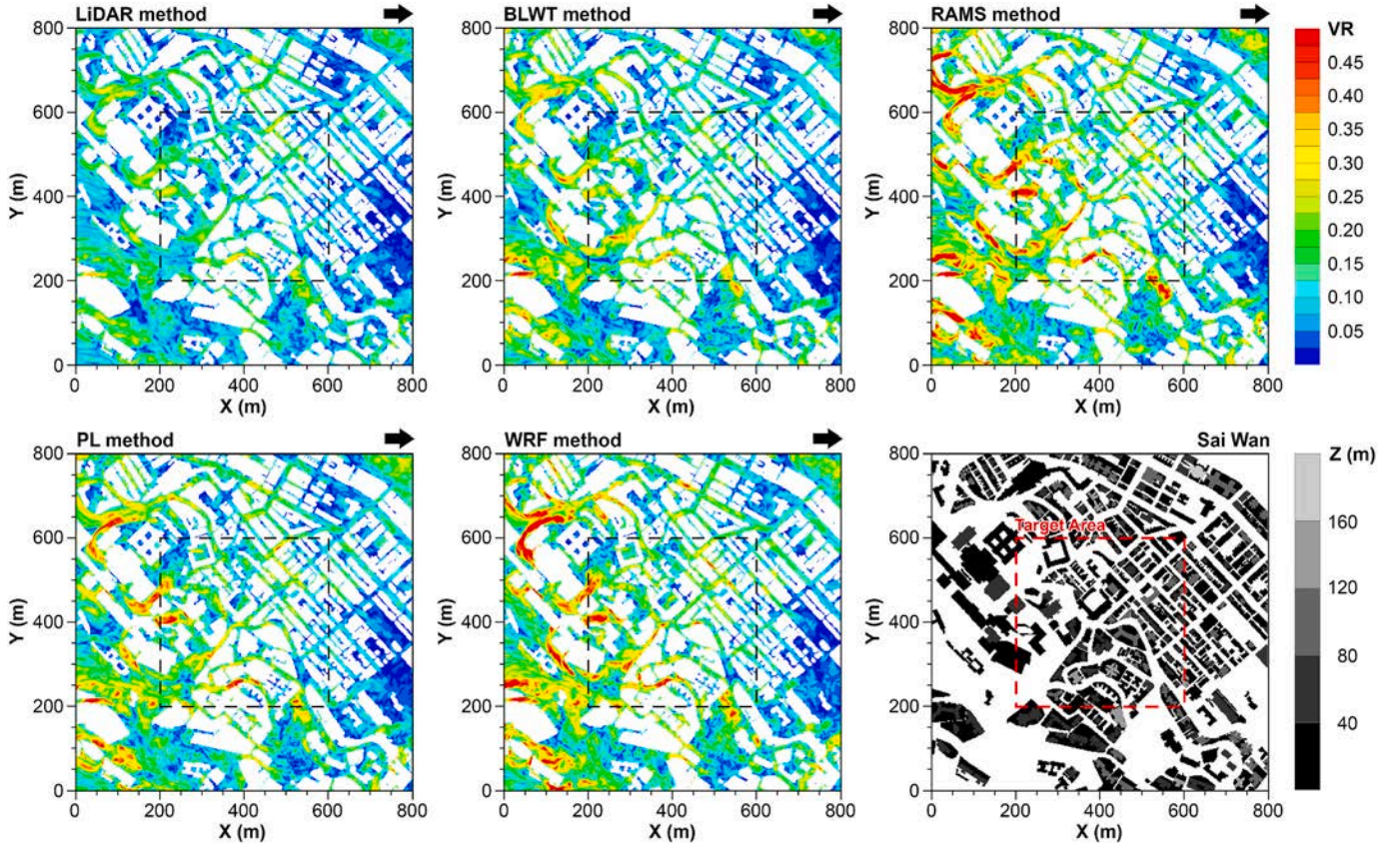
Fig. 9. Contours of pedestrian-level (Z = 2 m) wind velocity ratio (*VR*) obtained by the LiDAR, as a benchmark, and conventional methods (BLWT, RAMS, PL and WRF) in Sai Wan.

5.2. Percentage deviations of wind performance at the pedestrian level

To conduct quantitative analysis, we applied the percentage deviation of wind velocity ratio (PD_{VR}) as the main indicator to quantify the deviations on pedestrian-level wind assessment caused by the inlet wind profiles by conventional methods. PD_{VR} is calculated as:

$$PD_{VR} = \frac{VR_{CONVL} - VR_{LiDAR}}{VR_{LiDAR}} \times 100\% \qquad (6)$$

where VR_{CONVL} and VR_{LiDAR} denote the spatially-averaged wind velocity ratio from CFD simulations using the inlet wind profiles from conventional and LiDAR methods, respectively.

More than PD_{VR} for urban ventilation simulations, we also used wind speed frequency (PD_F) to quantify the deviations on outdoor thermal comfort assessment (i.e., the impact of wind speed on thermal comfort). They are calculated as:

$$PD_F = \frac{F_{CONVL} - F_{LiDAR}}{F_{LiDAR}} \times 100\% \qquad (7)$$

where F_{CONVL} and F_{LiDAR} denote the corresponding wind speed frequency from the CFD simulations. The calculation of the above two indicators was conducted at the target area of 400 m (X) × 400 m (Y) of the test sites, as shown in Figs. 9 and 10.

The results of PD_{VR} at the pedestrian level are shown in Fig. 11. In Sai Wan, both mesoscale meteorological modeling methods (RAMS and WRF) overestimate *VR* by around 65%. Smaller overestimations were observed in the BLWT and PL methods, but overestimations still reach over 25% and 40%, respectively. In Sai Kung, significant deviations were only observed in the BLWT and WRF methods, reaching around 10% and 20%, respectively. The deviations in the RAMS and PL methods are below 3%. The different results at two urban sites with different

densities, i.e., Sai Wan and Sai Kung, suggest that the conventional methods to reproduce inlet wind profiles for urban ventilation simulations are not acceptable at urban areas with higher building density and more heterogeneous surface morphologies.

The accurate prediction of wind speed is important as a factor of outdoor thermal comfort. Hence, a further analysis is given to PD_F by categorizing the pedestrian-level wind speed into three ranges: poor (≤0.3 m/s), medium (0.3–1.3 m/s), and comfort (>1.3 m/s). This wind-relevant criterion for outdoor thermal comfort was established by Yuan and Ng (2012), with reference to the findings in thermal comfort surveys (Cheng and Ng, 2006; Ng et al., 2008) in Hong Kong. As depicted in Fig. 12, the conventional methods overestimate the pedestrian-level wind speed of the comfort zone (i.e., PL and WRF >100%; BLWT around 80%; and RAMS around 40%) at an urban site with higher density (i.e. Sai Wan). On the other hand, the conventional methods overestimate the pedestrian-level wind speed of the poor zone (i.e., BLWT, RAMS, and PL > 50%) at the site with lower density (i.e. Sai Kung). The above analysis indicates that the conventional methods wrongly identify the zones with the poor or comfort wind speed of an urban site. The revealed deviations may mislead the wind-adaptive urban planning/design for improving the thermal environment. F_{LiDAR} and F_{CONVL} for calculating PD_F are provided in Table 3.

5.3. Percentage deviations of wind performance at the upper levels (0–60 m)

Given the importance of outdoor wind potential in street canyons on indoor natural ventilation, PD_{VR} values at upper levels are shown in Fig. 13. At the height of 0 m–60 m, where the urban canopy layer in Hong Kong is located (Ng et al., 2011), the deviations of all conventional methods are basically in line with the results at the pedestrian level, as
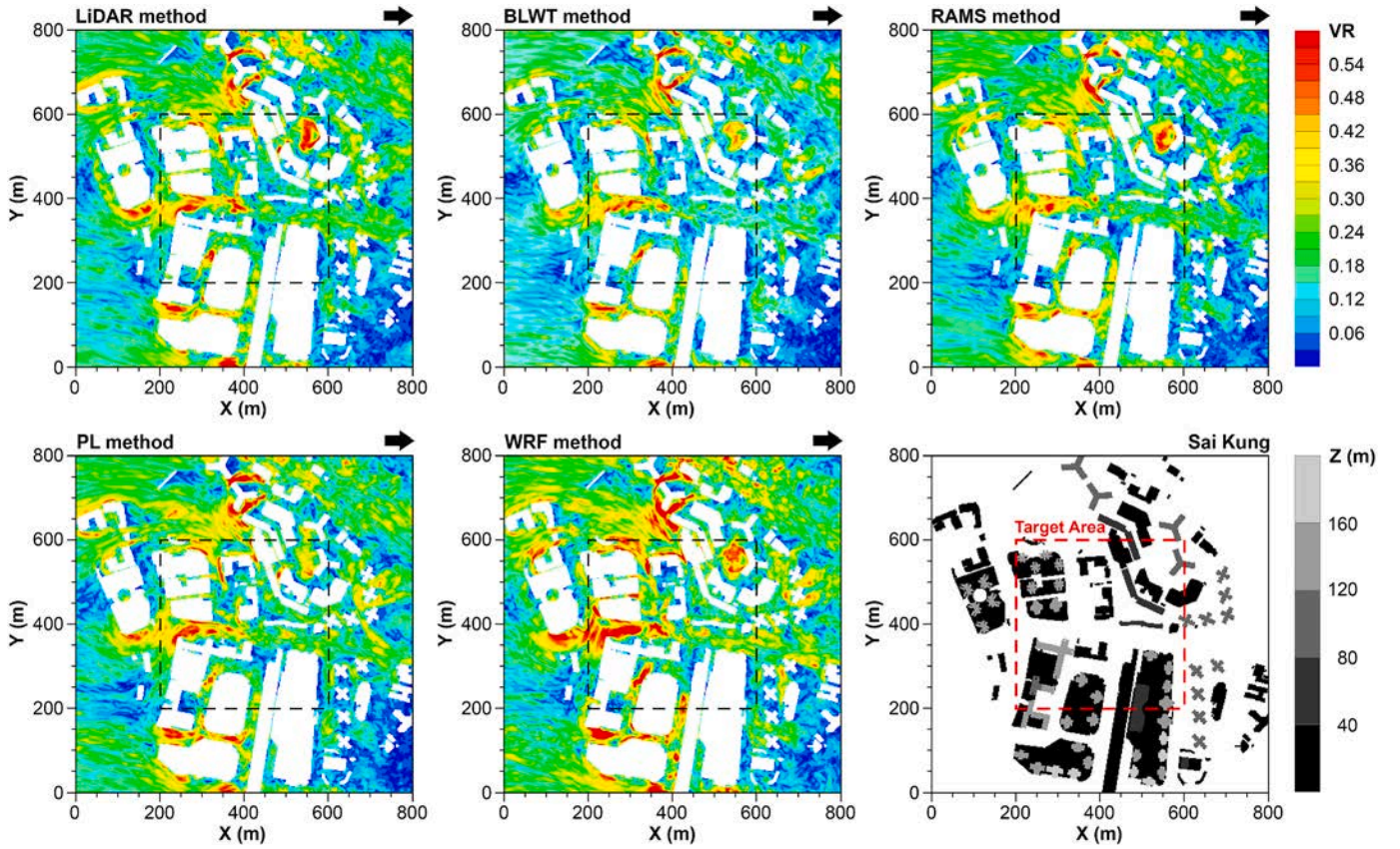
Fig. 10. Contours of pedestrian-level (Z = 2 m) wind velocity ratio (*VR*) obtained by the LiDAR and conventional methods (BLWT, RAMS, PL and WRF) in Sai Kung.
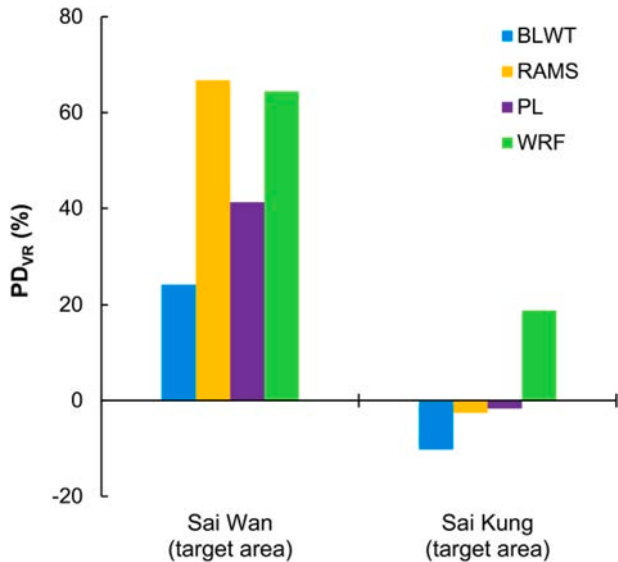

Fig. 11. Percentage deviation of pedestrian-level wind velocity ratio (*PD_VR*) of the conventional methods (BLWT, RAMS, PL and WRF) from the LiDAR method in Sai Wan and Sai Kung.

shown in Fig. 11. Most of the deviations at the site with higher density are significant (i.e., deviation >50%). However, the results for the site with lower density are acceptable. All deviations are less than 25%. It could be attributed to the less impact of urban morphology on air flow at lower density areas.

Overall, the results of PD_{VR} indicate more significant deviations of the conventional methods within the urban canopy layer (0–60 m) of an

urban site with a higher density. The deviations are induced by the inaccurate predictions of both the shapes of wind profiles and the incoming wind scale of U_∞, as mentioned in Section 3.3. It implies that the predictions of the near-ground flow behaviors are the most challenging, especially when the mechanical and thermal effects are significant (Wang et al., 2021).

5.4. Final evaluation and discussion of the conventional methods

The results in Sections 5.1–5.3 suggest significant deviations of all conventional methods for assessing near-ground ventilation at high-density urban sites. Overall, their deviations are summarized in an ascending order (Figs. 11 and 13): mesoscale meteorological modeling methods (RAMS and WRF), empirical modeling method (PL), and physical modeling method (BLWT). Amongst them, the PL method strikes the best balance between accuracy and data availability, and is the optimal option for estimating wind profiles when wind LiDAR observation is not available. The advantage of this method is that it on one hand has a relatively high accuracy. On the other hand, it is capable to estimate seasonal-averaged wind profiles over a city's whole territory with a simple formula. However, the PL method is found to perform worse at the urban site with higher density. This implies the need to establish a more explicit classification of aerodynamic roughness parameters for high-density urban terrain (i.e. more than two categories of cities and city centers (AIJ, 1996; Wieringa, 1992)). The BLWT method has the lowest deviations, but it turns out to be a secondary option due to its limitation in data availability. In the existing site wind availability data, the BLWT wind profiles are available at a limited number of sites of the city (PlanD, 2013a). The RAMS and WRF methods are the last option so far. The mesoscale meteorological modeling method has been used most frequently since it (i.e. RAMS) is a default method suggested by AVA to provide wind profiles for the whole territory (PlanD, 2013a).
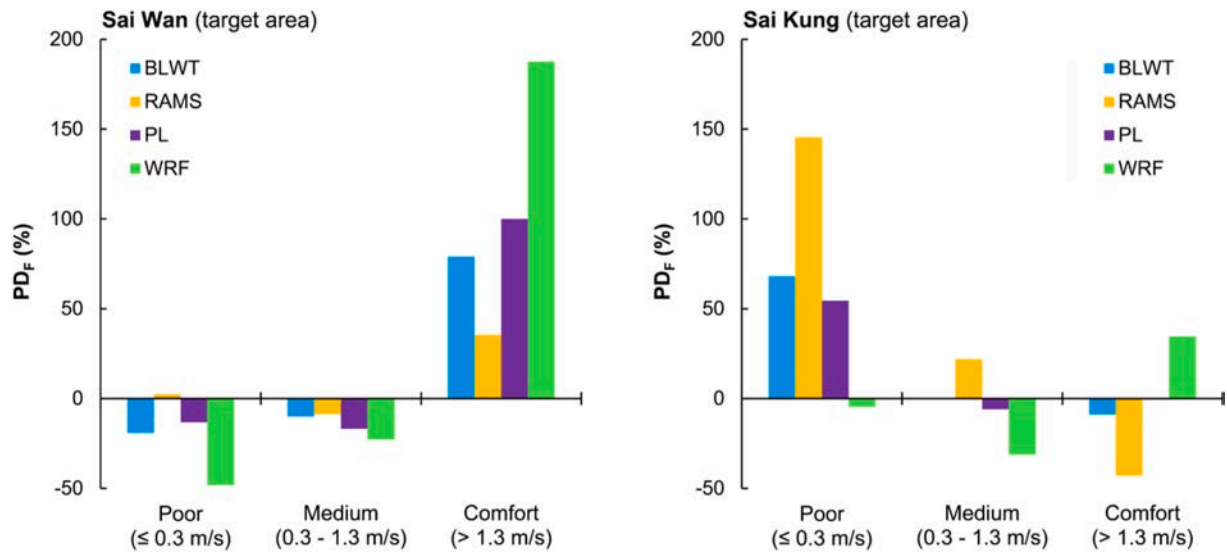
Fig. 12. Percentage deviation of pedestrian-level wind speed frequency (PD_F) of the conventional methods (BLWT, RAMS, PL and WRF) from the LiDAR method at three ranges of wind comfort (Yuan and Ng, 2012) in Sai Wan and Sai Kung.

Table 3
Pedestrian-level wind speed frequency (%) obtained by the LiDAR and conventional methods (BLWT, RAMS, PL and WRF) in Sai Wan and Sai Kung.

Method	Sai Wan			Sai Kung		
	Poor	Medium	Comfort	Poor	Medium	Comfort
LiDAR	23.7	62.6	13.7	5.9	49.1	45.0
BLWT	19.1	56.3	24.6	9.9	49.1	41.0
RAMS	24.3	57.1	18.6	14.5	59.8	25.7
PL	20.6	52.0	27.4	9.1	46.1	44.8
WRF	12.3	48.3	39.4	5.6	33.8	60.6

However, the large deviations of this method, as revealed in this study, are incompatible with their high frequency of use in practice. In this regard, an optimization of this method is required in the near future.

6. Conclusions

This study evaluates the accuracy of the incoming wind profiles estimated by various conventional methods as inflow boundary condition, and the impact on numerical simulation results for urban ventilation assessment, by using Light Detection and Ranging (LiDAR) observation as a benchmark. The conventional methods include the Boundary Layer Wind Tunnel (BLWT), Regional Atmospheric Modeling System (RAMS), Weather Research and Forecasting (WRF), Power Law (PL) and methods. We select two typical high-density urban sites for evaluation from a downtown district (Sai Wan) and a new town district (Sai Kung) in Hong Kong. The evaluation focuses on the summer prevailing southwest wind condition to address the "high-temperature and weak-wind" problem. CFD simulations are conducted by LES model to evaluate the sensitivity of urban ventilation assessment results to the deviations on wind profiles. The cross-comparison results indicate significant deviations of wind profiles estimated by the conventional
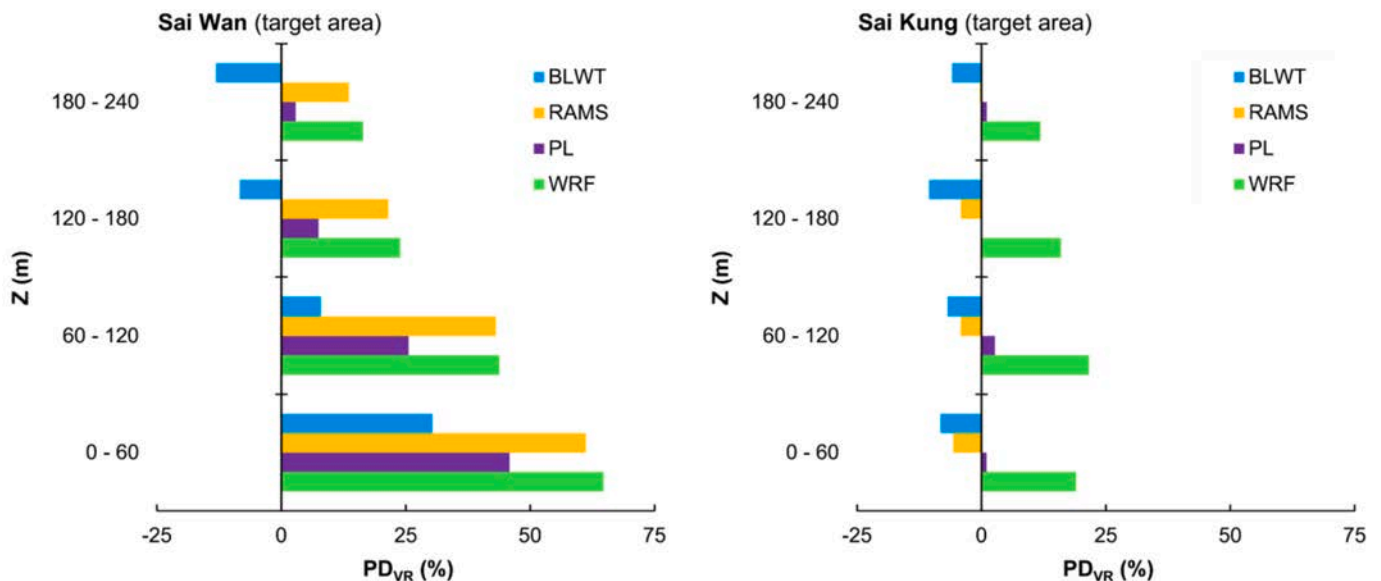
Fig. 13. Percentage deviation of wind velocity ratio (PD_{VR}) at different upper levels of the conventional methods (BLWT, RAMS, PL and WRF) from the LiDAR method in Sai Wan and Sai Kung.

methods, and more importantly, the CFD simulation results indicate that the deviations on wind profiles cause even bigger overestimations or underestimations on pedestrian-level wind assessment. Key findings are summarized as follows:

● Incoming wind profiles established by conventional methods are significantly different with the one measured by LiDAR. But the deviations of vertical wind velocity ratio (VR) profiles from LiDAR measurement are much smaller than the ones of the wind profile itself, especially the VR profile by PL method at the lower density urban area (i.e., Sai Kung in Fig. 5).

● Incoming wind profiles by conventional methods lead to significant deviations of pedestrian-level VR in CFD simulation. The largest deviations are found in the mesoscale meteorological modeling methods (i.e., RAMS and WRF (>65%)), following by empirical PL model (>40%) and physical BLWT model (>25%). Significant deviations of VR within the urban canopy layer (0–60m) are also observed.

● CFD simulation results with incoming wind profiles by conventional methods wrongly identify the zones with the poor and comfort wind speed at the pedestrian level of a high-density urban site, with the deviations of over 100%. Smaller deviations are found at the urban site with lower density than higher density.

● Given identified deviations caused by all the conventional methods, the incoming wind profile directly measured by LiDAR is recommended at the ventilation assessment in the future, especially for new important projects.

● Among conventional methods, the CFD simulation using the wind profile from wind tunnel experiment (BLWT) causes lowest deviation from the one using LiDAR wind profile.

● Based on the cross-comparison results, the PL method achieves the best balance between accuracy and data availability. Therefore, PL method is identified as the optimal practical option for estimating wind profiles when LiDAR observation and wind tunnel data are not available.

The findings in this paper imply a need of long-term wind LiDAR observation at high-density urban areas to provide more reliable input wind profiles to urban ventilation assessment. The accuracy of assessment results is crucial to the decision making in the wind-oriented urban planning/design especially during weak wind periods. The findings also imply a critical need to optimize the conventional methods to reproduce the wind profiles when wind LiDAR is not available. Given that the conventional methods tested in this study are used worldwide, the current findings will be a valuable reference to the optimization of urban ventilation assessment not only in Hong Kong but also in other high-density cities.

7. Limitations and future works

This paper is known to have limitations. Firstly, the wind LiDAR fails to provide near-ground wind speed data due to their technical limitation and there is no available weather station near the LiDAR sites. However, these measurement data are needed to complete the observed wind profiles and validations of the conventional methods. The near-ground wind speed measurement data are also crucial for validating the CFD simulation results within the city in the future. Secondly, the wind LiDAR only provides data at a vertical line instead of a vertical surface, while a further investigation is necessary to identify the wind variation at the vertical surface and provide more comprehensive inlet wind conditions to a particular urban site. Thirdly, the cartesian grids used in this study make segmentation of the oblique building facades which can cause different separations of the flow around buildings with respect to reality or higher resolved geometry/grids, while structured grids with higher resolutions should be used to more accurately simulate the flow behaviors if more computational power is granted. Finally, the current evaluation is conducted at only two typical urban sites with relatively flat terrain, while a network of wind LiDAR is expected to be established in Hong Kong. It could provide a more explicit investigation of wind characteristics over different terrain such as mountainous terrain which is abundant in Hong Kong and can considerably modify the local wind as demonstrated by Tse et al. (2016) and An et al. (2020).

Appendix A. DBS scan mode of wind LiDAR

During the field observation of wind LiDAR, laser beams with an eye-safe wavelength of 1.54 μm were emitted and received cyclically at five directions, namely, the east-tilted, south-tilted, west-tilted, north-tilted and vertical directions. The radical wind speed at each height was calculated proportionally to the detected Δf, and then converted into the horizontal components of the wind speed at the corresponding height, as shown in Fig. 14, by the following equations:

$$u_{EW} = 0.5(V_{RE} - V_{RW})/\sin\gamma \tag{8}$$

$$u_{NS} = 0.5(V_{RN} - V_{RS})/\sin\gamma \tag{9}$$

$$U = \sqrt{u_{EW}^2 + u_{NS}^2} \tag{10}$$

where u_{EW} and u_{NS} refer to the east-west and north-south horizontal components of the wind speed, respectively; V_{RE}, V_{RW}, V_{RN} and V_{RS} refer to the radial wind speed along the east-tilted, west-tilted, north-tilted and south-tilted directions, respectively; γ refers to the half cone angle (15°). The measurement accuracy of the radial wind speed of WindCube 100S is reported to be 0.5 m/s at the range between 0 and 115 m/s (Vaisala, 2021).
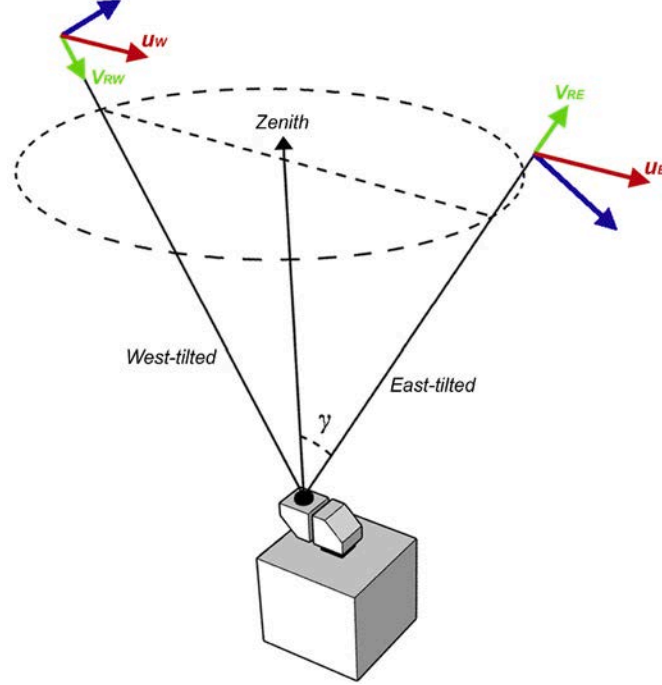

Fig. 14. Diagram of the detections of the radial wind speed along the east-tilted (V_{RE}) and west-tilted (V_{RW}) directions, as well as their conversions into the east-west horizontal component of the wind speed (u_{EW}).

Appendix B. Wind LiDAR validation

The two wind LiDAR have been calibrated by the manufacturer with a certified wind LiDAR ($R^2 = 0.99$) before their on-site installations. To balance the data quality and data availability in local weather conditions, the minimum threshold of the carrier-to-noise ratio was set to be -27 dB (He et al., 2021). For on-site validation purpose, as shown in Fig. 15a, one of the wind LiDAR was placed at the King's Park meteorological station, next to the HKO automatic upper-air sounding system, which is the only source of balloon-based vertical wind measurements in Hong Kong. In the sounding system, the launched radiosondes measure the vertical wind speed profiles at 8 a.m. and 8 p.m. daily (HKO, 2021c). To align with the sounding data, the hourly-averaged wind speed profiles measured by the wind LiDAR at the same time were used in the validation. Fig. 15b shows the validation results in terms of the vertical profiles of horizontal wind speed and direction in a period of two weeks. It presents a strong agreement between the wind LiDAR and sounding data, where R^2 reaches 0.88 and 0.82 for wind speed and direction, respectively.
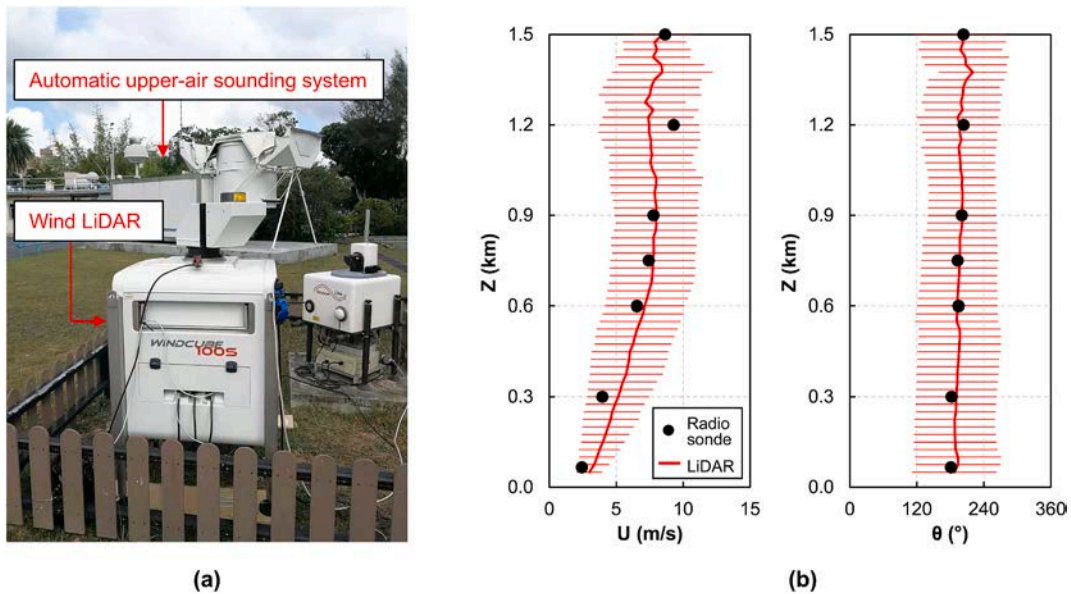

Fig. 15. Wind LiDAR on-site validation: (a) a wind LiDAR versus the radiosondes of the HKO automatic upper-air sounding system at the King's Park meteorological station; and (b) their comparison results of the hourly-averaged vertical profiles of horizontal wind speed (U) and direction (θ) (i.e., mean and standard deviations) in a period of two weeks.

Appendix C. Diagram of wind tunnel facility

The low-speed wind tunnel facility for developing the BLWT wind profiles has a test section of 40 m (length) × 5 m (width) × 4 m (height), as shown in Fig. 16. In an experiment, the wind characteristics at the inlet of the facility were calibrated against target wind speed and turbulence intensity profiles by adjusting the combinations of spires, grids, fences and roughness elements. The reported error in the calibration was within ±10% (PlanD, 2013a).
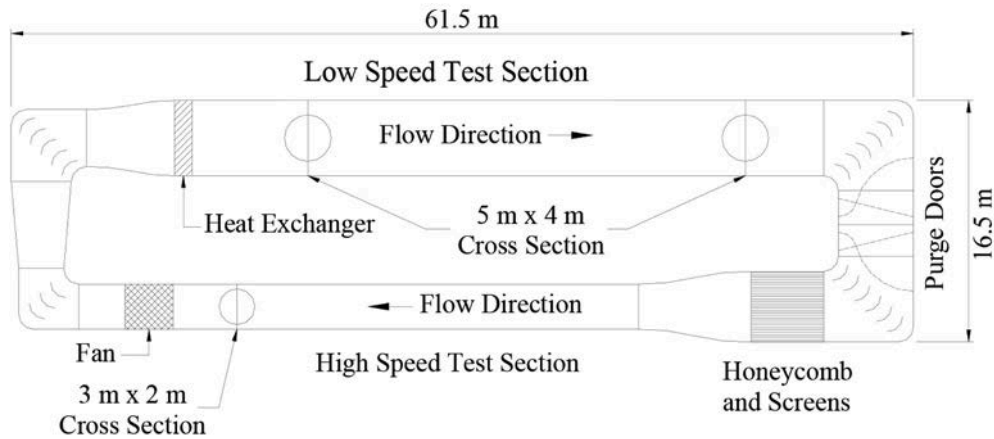

Fig. 16. Diagram of the low-speed wind tunnel facility for developing the BLWT wind profiles (PlanD, 2013a).

Appendix D. LES validation

This study used two sets of wind tunnel experimental data to validate the accuracy of PALM at the pedestrian level. As shown in Fig. 17, the first wind tunnel dataset was provided by the AIJ (MENG and HIBI, 1998) using a single generic building, whose full-scale size was prescribed to be 16 m (X) × 16 m (Y) × 32 m (Z) in this study. The second wind tunnel dataset was provided by the School of Architecture, the Chinese University of Hong Kong (PlanD, 2010) using a realistic urban site, which is the same as the AVA test site in Sai Kung in this paper. Since the topography model was not taken into account in the simulations, the validation selected the experimental data measured under the northwest wind direction, where the upwind side of the urban model was flat and had no blockage of mountain.
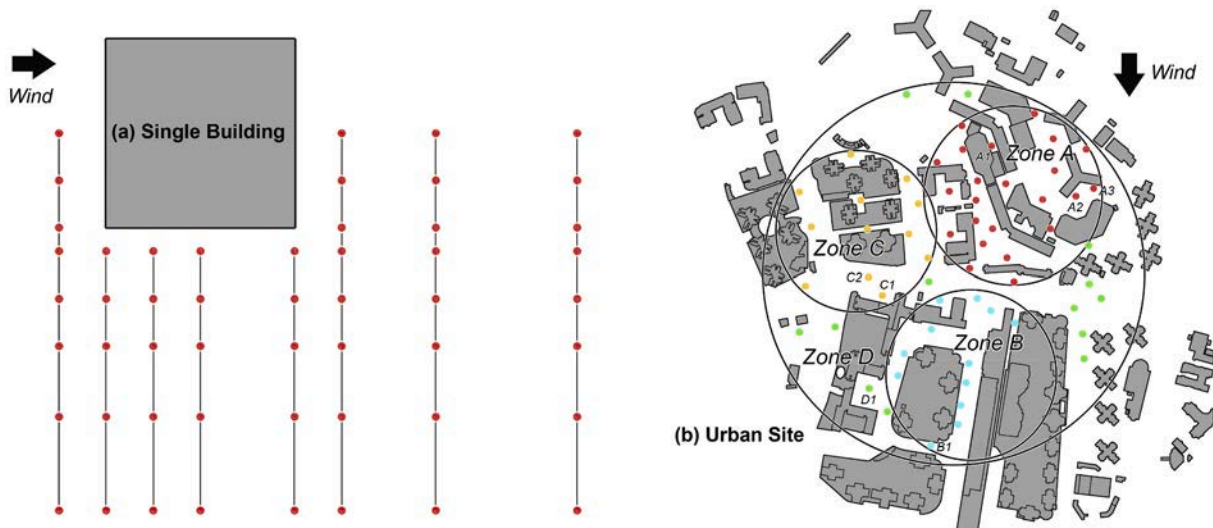

Fig. 17. Wind tunnel physical models and their measuring points in the LES validations: (a) a generic single building model from the AIJ (MENG and HIBI, 1998); and (b) a realistic urban model in Sai Kung, Hong Kong from the School of Architecture, the Chinese University of Hong Kong (PlanD, 2010).

In the validation results, as shown in Fig. 18, the simulated data fairly agrees with the experimental data with a single building, where R^2 reaches above 0.9. However, when more uncertainties were introduced in the validation with an urban model, the deviations become larger, with R^2 reaching just below 0.7. These uncertainties can be from either the experiments or simulations. In the experiments, for example, the hot-wire sensors used for measuring wind speed have been known to have limitations at the close proximity of buildings with intensive turbulence (Blocken et al., 2016). Besides, the positions of the measuring points in a complex urban model may be recorded with deviations due to human error (Wang et al., 2020). In the simulations, for example, the widely-used CFD models, RANS and LES, cannot fully resolve the turbulent flow due to the limited computational power (Blocken, 2014). The cartesian computational grids make segmentation of the building facades that are oblique to X and Y directions, and can cause different separations of the flow around the buildings and potential discretization errors with respect to reality or higher resolved geometry/grids. Additionally, the realistic background conditions in the wind tunnel, such as temperature, cannot be fully replicated in the simulations due to the lack of information. These uncertainties usually lead to worse agreements between the CFD and wind tunnel results with an urban model

than a single building (Tachibana et al., 2017; Tominaga et al., 2005). In the current validation result, most of the test points have the deviations of below or around 30%, while those outliers are mainly located at the areas sheltered by buildings at the windward side (Fig. 17), which is in line with the previous validation results with PALM (Gronemeier et al., 2020; Wang et al., 2020). Given that the focus of this study is on the spatially-averaged wind performance of an urban site and the validation result of *VR* frequency is fairly good (Fig. 19), the current LES model is considered reliable to be applied in a high-density urban model.
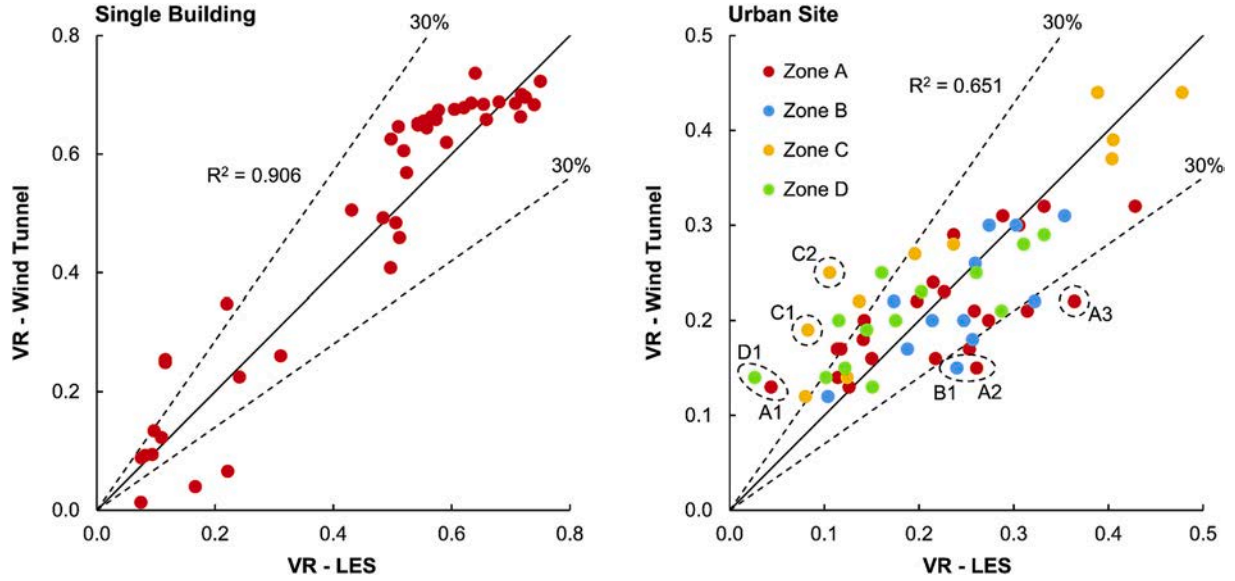

Fig. 18. Comparisons between wind tunnel and LES results in terms of pedestrian-level wind velocity ratio (*VR*) in the validations with a generic single building and a realistic urban site (zones A, B, C and D).
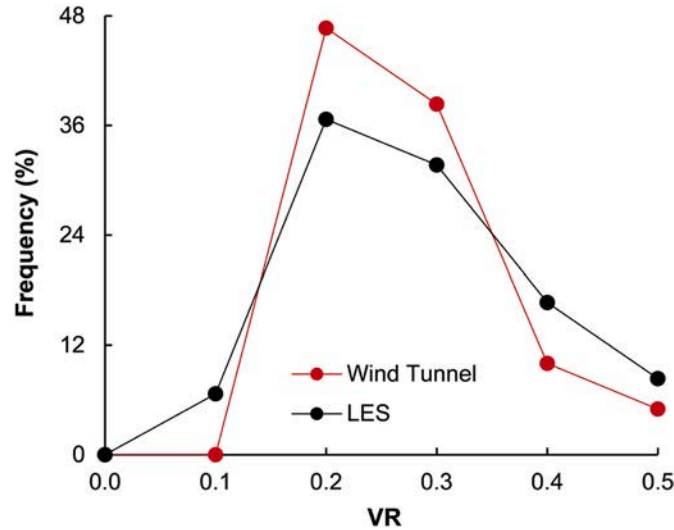

Fig. 19. Comparisons between wind tunnel and LES results in terms of frequency of pedestrian-level wind velocity ratio (*VR*) in the validation with a realistic urban site.

Appendix E. LES sensitivity test on inlet wind profile

The LiDAR wind speed profile in Sai Wan was tested in an empty domain to identify the horizontal inhomogeneity phenomenon (Blocken et al., 2007) during the profile development. As shown in Fig. 20, the near-ground part (i.e., $Z = 0$–15 m) of the inlet wind profile decreases significantly from the inlet to incident positions (i.e., the leeward side of the urban model) due to the wall-function roughness modifications, while the upper part within the urban canopy layer (i.e., $Z = 15$–60 m) remains almost unchanged and consistent with heights. The characteristics of the incident wind profile agrees the reality described in Fig. 1 according to Oke (2004), and Bentham and Britter (2003), hench fulfilling the assumption in this paper.
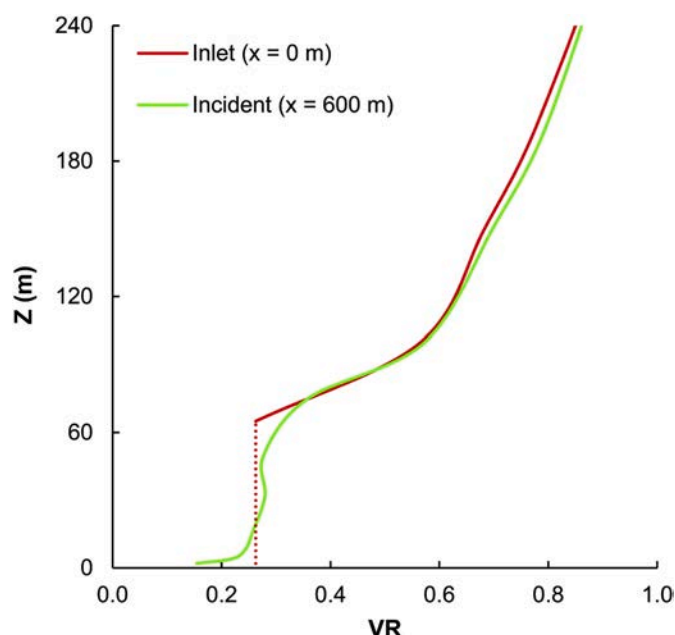
Fig. 20. Development of an inlet wind profile (i.e., the LiDAR wind speed profile in Sai Wan) from the inlet to incident positions in an empty domain.

References

Abbas, G.M., Dino, I.G., 2021. The Impact of Natural Ventilation on Airborne Biocontaminants: a Study on COVID-19 Dispersion in an Open Office. Construction and Architectural Management, Engineering.

An, K., Wong, S.-M., Fung, J.C.H., Ng, E., 2020. Revisit of prevailing practice guidelines and investigation of topographical treatment techniques in CFD-Based air ventilation assessments. Build. Environ. 169, 106580.

Architectural Institute of Japan (AIJ), 1996. AIJ Recommendations for Loads on Buildings. AIJ, Japan.

Australian Institute of Architects, 2021. The Lord Mayor's Brisbane Buildings that Breathes. Australian Institute of Architects, Australia.. Available from: https://www.architecture.com.au/. (Accessed 15 July 2021)

Barlow, J.F., 2014. Progress in observing and modelling the urban boundary layer. Urban Clim. 10, 216–240.

Barlow, J.F., Dunbar, T., Nemitz, E., Wood, C.R., Gallagher, M., Davies, F., O'Connor, E., Harrison, R., 2011. Boundary layer dynamics over London, UK, as observed using Doppler lidar during REPARTEE-II. Atmos. Chem. Phys. 11 (5), 2111–2125.

Bentham, T., Britter, R., 2003. Spatially averaged flow within obstacle arrays. Atmos. Environ. 37 (15), 2037–2043.

Blocken, B., 2014. 50 years of computational wind engineering: past, present and future. J. Wind Eng. Ind. Aerod. 129, 69–102.

Blocken, B., Stathopoulos, T., Carmeliet, J., 2007. CFD simulation of the atmospheric boundary layer: wall function problems. Atmos. Environ. 41 (2), 238–252.

Blocken, B., Defraeye, T., Derome, D., Carmeliet, J., 2009. High-resolution CFD simulations for forced convective heat transfer coefficients at the facade of a low-rise building. Build. Environ. 44 (12), 2396–2412.

Blocken, B., Stathopoulos, T., Van Beeck, J., 2016. Pedestrian-level wind conditions around buildings: review of wind-tunnel and CFD techniques and their accuracy for wind comfort assessment. Build. Environ. 100, 50–81.

Cheng, V., Ng, E., 2006. Thermal comfort in urban open spaces for Hong Kong. Architect. Sci. Rev. 49 (3), 236–242.

Counihan, J., 1975. Adiabatic atmospheric boundary layers: a review and analysis of data from the period 1880–1972. Atmos. Environ. 9 (10), 871–905.

Davenport, A.G., 1967. Gust loading factors. J. Struct. Div. 93 (3), 11–34.

Deaves, D., Harris, R., 1978. A Mathematical Model of the Structure of Strong Winds. Construction Industry Research and Information Association Report Number 76. CIRIA, London, England.

Drew, D.R., Barlow, J.F., Lane, S.E., 2013. Observations of wind speed profiles over Greater London, UK, using a Doppler lidar. J. Wind Eng. Ind. Aerod. 121, 98–105.

Engineering Sciences Data Unit, 1985. Data Item 85020: Characteristics of Atmospheric Turbulence Near the Ground. Engineering Sciences Data Unit, UK.

Gronemeier, T., Raasch, S., Ng, E., 2017. Effects of unstable stratification on ventilation in Hong Kong. Atmosphere 8 (9), 168.

Gronemeier, T., Surm, K., Harms, F., Leitl, B., Maronga, B., Raasch, S., 2020. Validation of the dynamic core of the PALM model system 6.0 in urban environments: LES and wind-tunnel experiments. Geosci. Model Dev. Discuss. (GMDD) 1–26.

Gryning, S.-E., Batchvarova, E., Brümmer, B., Jørgensen, H., Larsen, S., 2007. On the extension of the wind profile over homogeneous terrain beyond the surface boundary layer. Boundary-Layer Meteorol. 124 (2), 251–268.

Gryning, S.-E., Batchvarova, E., Quante, M., Matthias, V., 2011. Evaluation of vertical profiles in mesoscale meteorological models based on observations for the COST728 study of winter 2003 PM episodes in Europe. In: Air Pollution Modeling and its Application XXI. Springer, pp. 499–503.

Haman, C.L., Lefer, B., Morris, G.A., 2012. Seasonal variability in the diurnal evolution of the boundary layer in a near-coastal urban environment. J. Atmos. Ocean. Technol. 29 (5), 697–710.

He, Y., Tablada, A., Wong, N.H., 2018. Effects of non-uniform and orthogonal breezeway networks on pedestrian ventilation in Singapore's high-density urban environments. Urban Clim. 24, 460–484.

He, Y., Tablada, A., Wong, N.H., 2019. A parametric study of angular road patterns on pedestrian ventilation in high-density urban areas. Build. Environ. 151, 251–267.

He, Y., Ren, C., Mak, H.W.L., Lin, C., Wang, Z., Fung, J.C.H., Li, Y., Lau, A.K.H., Ng, E., 2021. Investigations of high-density urban boundary layer under summer prevailing wind conditions with Doppler LiDAR: a case study in Hong Kong. Urban Clim. 38, 100884.

He, Y., Yuan, C., Ren, C., Wang, W., Shi, Y., Ng, E., 2022a. Urban ventilation assessment with improved vertical wind profile in high-density cities–Investigations in nighttime extreme heat. Build. Environ. 216, 109018.

He, Y., Tablada, A., Deng, J.Y., Shi, Y., Wong, N.H., Ng, E., 2022b. Linking of pedestrian spaces to optimize outdoor air ventilation and quality in tropical high-density urban areas. Urban Clim.

Heus, T., van Heerwaarden, C.C., Jonker, H.J., Siebesma, A.P., Axelsen, S., van den Dries, K., Geoffroy, O., Moene, A.F., Pino, D., de Roode, S., 2010. Formulation of and numerical studies with the Dutch atmospheric large-eddy simulation (DALES). Geosci. Model Dev. (GMD) 3, 415–444.

HKO, 2021a. Number of Hot Nights Observed at the Hong Kong Observatory since 1884 [cited. https://www.hko.gov.hk/en/cis/statistic/hngtday_statistic.htm. (Accessed 15 July 2021). Available from:

HKO, 2021b. Climatological Database [cited. https://www.hko.gov.hk/en/cis/climat.htm. (Accessed 15 July 2021). Available from:

HKO, 2021c. Upper-air Weather Measurements in Hong Kong [cited. https://www.hko.gov.hk/en/wservice/tsheet/uamet.htm. (Accessed 15 July 2021). Available from:

Housing, Planning and Lands Bureau (HPLB) and Environment, Transport and Works Bureau (ETWB), 2006. Technical Circular NO. 1/06: Air Ventilation Assessments. HPLB and ETWB, Hong Kong.

Hu, X.-M., Nielsen-Gammon, J.W., Zhang, F., 2010. Evaluation of three planetary boundary layer schemes in the WRF model. J. Appl. Meteorol. Climatol. 49 (9), 1831–1844.

Huang, M., Gao, Z., Miao, S., Chen, F., LeMone, M.A., Li, J., Hu, F., Wang, L., 2017. Estimate of boundary-layer depth over Beijing, China, using Doppler lidar data during SURF-2015. Boundary-Layer Meteorol. 162 (3), 503–522.

Institute for the Environment (IENV), 2021. HKUST Real Time MM5/WRF Simulations. IENV, the Hong Kong University of Science and Technology, Hong Kong.

Irwin, J.S., 1967. A theoretical variation of the wind profile power-law exponent as a function of surface roughness and stability. Atmos. Environ. 13 (1), 191–194, 1979.

Kent, C.W., Grimmond, C.S.B., Gatey, D., Barlow, J.F., 2018. Assessing methods to extrapolate the vertical wind-speed profile from surface observations in a city centre during strong winds. J. Wind Eng. Ind. Aerod. 173, 100–111.

Kikumoto, H., Ooka, R., Sugawara, H., Lim, J., 2017. Observational study of power-law approximation of wind profiles within an urban boundary layer for various wind conditions. J. Wind Eng. Ind. Aerod. 164, 13–21.

Kotthaus, S., Halios, C.H., Barlow, J.F., Grimmond, C., 2018. Volume for pollution dispersion: london's atmospheric boundary layer during ClearfLo observed with two ground-based lidar types. Atmos. Environ. 190, 401–414.

Lane, S., Barlow, J.F., Wood, C.R., 2013. An assessment of a three-beam Doppler lidar wind profiling method for use in urban areas. J. Wind Eng. Ind. Aerod. 119, 53–59.

Lettau, H., 1969. Note on aerodynamic roughness-parameter estimation on the basis of roughness-element description. J. Appl. Meteorol. 8 (5), 828–832.

Lim, J., Akashi, Y., Ooka, R., Kikumoto, H., Choi, Y., 2017. A probabilistic approach to the energy-saving potential of natural ventilation: effect of approximation method for approaching wind velocity. Build. Environ. 122, 94–104.

Maronga, B., Banzhaf, S., Burmeister, C., Esch, T., Forkel, R., Fröhlich, D., Fuka, V., Gehrke, K.F., Geletič, J., Giersch, S., 2020. Overview of the PALM model system 6.0. Geosci. Model Dev. (GMD) 13 (3), 1335–1372.

Martilli, A., 2007. Current research and future challenges in urban mesoscale modelling. Int. J. Climatol.: J. Royal Meteorol. Soc. 27 (14), 1909–1918.

Meng, Y., Hibi, K., 1998. Turbulent measurments of the flow field around a high-rise building. J. Wind Eng. 1998 (76), 55–64.

Menut, L., Flamant, C., Pelon, J., Flamant, P.H., 1999. Urban boundary-layer height determination from lidar measurements over the Paris area. Appl. Opt. 38 (6), 945–954.

Miguel, M., Hien, W.N., Marcel, I., Chung, H.D.J., Yueer, H., Zhonqi, Y., Ji-Yu, D., Raghavan, S.V., Son, N.N., 2021. A physically-based model of interactions between a building and its outdoor conditions at the urban microscale. Energy Build. 237, 110788.

National University of Singapore, 2021. Urban Climatic Mapping Studies for Singapore. National University of Singapore, Singapore. Available from: https://cde.nus.edu.sg/csac/research/urban-climatic-mapping-studies-for-singapore/. (Accessed 15 July 2021).

Ng, E., 2009. Policies and technical guidelines for urban planning of high-density cities–air ventilation assessment (AVA) of Hong Kong. Build. Environ. 44 (7), 1478–1488.

Ng, E., Chan, C., Cheng, V., 2008. Urban Climatic Map and Standards for Wind Environment - Feasibility Study. Technical Input Report No.1: Methodologies and Findings of User's Wind Comfort Level Survey. Planning Department, Hong Kong.

Ng, E., Yuan, C., Chen, L., Ren, C., Fung, J.C., 2011. Improving the wind environment in high-density cities by understanding urban morphology and surface roughness: a study in Hong Kong. Landsc. Urban Plann. 101 (1), 59–74.

Nikkho, S.K., Heidarinejad, M., Liu, J., Srebric, J., 2017. Quantifying the impact of urban wind sheltering on the building energy consumption. Appl. Therm. Eng. 116, 850–865.

Oke, T.R., 2004. Initial Guidance to Obtain Representative Meteorological Observations at Urban Sites, Instruments and Observing Methods. World Meteorological Organization. *Report No. 81*.

PALM group, 2022. Topography Data, Input and Output Files. Institute of Meteorology and Climatology of Leibniz Universität Hannover, Germany. Available from: https://palm.muk.uni-hannover.de/trac/wiki/doc/app/iofiles#TOPOGRAPHY_DATA. (Accessed 15 July 2022).

Palyvos, J., 2008. A survey of wind convection coefficient correlations for building envelope energy systems' modeling. Appl. Therm. Eng. 28 (8–9), 801–808.

Park, M.-S., Chae, J.-H., 2018. Features of sea–land-breeze circulation over the seoul metropolitan area. Geosci. Lett. 5 (1), 1–12.

Pielke Sr, R.A., 2013. Mesoscale Meteorological Modeling. Academic press.

PlanD, 2013a. Site Wind Availability Data. PlanD, Hong Kong.. Available from: https://www.pland.gov.hk/pland_en/info_serv/site_wind/index.html. (Accessed 15 July 2021)

PlanD, 2013b. Final report: Site wind availability system and web-based site wind availability database, consultancy study on establishment of simulated site wind availability data for air ventilation assessments in Hong Kong. PlanD, Hong Kong.

Planning Department (PlanD), 2010. Working Paper 2C: Wind Tunnel Benchmarking Studies – Batch II, Urban Climatic Map and Standards for Wind Environment – Feasibility Study. PlanD, Hong Kong.

Ren, C., Yang, R., Cheng, C., Xing, P., Fang, X., Zhang, S., Wang, H., Shi, Y., Zhang, X., Kwok, Y.T., 2018. Creating breathing cities by adopting urban ventilation assessment and wind corridor plan–the implementation in Chinese cities. J. Wind Eng. Ind. Aerod. 182, 170–188.

Resler, J., Eben, K., Geletič, J., Krč, P., Rosecký, M., Sühring, M., Belda, M., Fuka, V., Halenka, T., Huszár, P., 2021. Validation of the PALM model system 6.0 in a real urban environment: a case study in Dejvice, Prague, the Czech Republic. Geosci. Model Dev. (GMD) 14 (8), 4797–4842.

Rossby, C.-G., Montgomery, R.B., 1935. The Layer of Frictional Influence in Wind and Ocean Currents.

Rotach, M.W., Gryning, S.E., Tassone, C., 1996. A two-dimensional Lagrangian stochastic dispersion model for daytime conditions. Q. J. R. Meteorol. Soc. 122 (530), 367–389.

Roth, M., 2000. Review of atmospheric turbulence over cities. Q. J. R. Meteorol. Soc. 126 (564), 941–990.

Salamanca, F., Krpo, A., Martilli, A., Clappier, A., 2010. A new building energy model coupled with an urban canopy parameterization for urban climate simulations—part I. formulation, verification, and sensitivity analysis of the model. Theor. Appl. Climatol. 99 (3), 331–344.

Salamanca, F., Martilli, A., Tewari, M., Chen, F., 2011. A study of the urban boundary layer using different urban parameterizations and high-resolution urban canopy parameters with WRF. J. Appl. Meteorol. Climatol. 50 (5), 1107–1128.

Sepe, V., Rizzo, F., Ricciardelli, F., Avossa, A., 2018. Characterization of mean wind profiles and surface roughness assessment from wind LIDAR measurements. In: Conference of the Italian Association for Wind Engineering. Springer.

Steeneveld, G., Tolk, L., Moene, A., Hartogensis, O., Peters, W., Holtslag, A., 2011. Confronting the WRF and RAMS mesoscale models with innovative observations in The Netherlands: evaluating the boundary layer heat budget. J. Geophys. Res. Atmos. 116 (D23).

Stull, R.B., 1988. An Introduction to Boundary Layer Meteorology, vol. 13. Springer Science & Business Media.

Sutton, O., 1947. The problem of diffusion in the lower atmosphere. Q. J. R. Meteorol. Soc. 73 (317-318), 257–281.

Tachibana, T., Miyashita, K., Kishida, T., Yoshie, R., Sasaki, R., 2017. Comparison of wind tunnel experiment and large eddy simulation results for pollutant dispersion in urban area. In: Annual Meeting Architectural Institute of Japan, vol. 2017, 41431.

Taylor, G.I., 1915. Eddy motion in the atmosphere. Phil. Trans. Roy. Soc. Lond. 215 (523–537), 1–26.

Tieben, H., Chu, J., Soares, N., Yiu, E., 2015. Environmental Urban design and planning rules and their impact on street spaces in Hong Kong and Macau. In: Proceedings of the 8th Conference International Forum on Urbanism. Citeseer, True Smart and Green City.

Tominaga, Y., Stathopoulos, T., 2018. CFD simulations of near-field pollutant dispersion with different plume buoyancies. Build. Environ. 131, 128–139.

Tominaga, Y., Yoshie, R., Mochida, A., Kataoka, H., Harimoto, K., Nozu, T., 2005. Cross comparisons of CFD prediction for wind environment at pedestrian level around buildings part 2: comparison of results for flowfield around building complex in actual urban area. In: The Sixth Asia-Pacific Conference on Wind Engineering, pp. 2661–2670. Seoul, Korea.

Tominaga, Y., Mochida, A., Yoshie, R., Kataoka, H., Nozu, T., Yoshikawa, M., Shirasawa, T., 2008. AIJ guidelines for practical applications of CFD to pedestrian wind environment around buildings. J. Wind Eng. Ind. Aerod. 96 (10–11), 1749–1761.

Tse, K.T., Weerasuriya, A.U., Kwok, K.C.S., 2016. Simulation of twisted wind flows in a boundary layer wind tunnel for pedestrian-level wind tunnel tests. J. Wind Eng. Ind. Aerod. 159, 99–109.

Uehara, K., Murakami, S., Oikawa, S., Wakamatsu, S., 2000. Wind tunnel experiments on how thermal stratification affects flow in and above urban street canyons. Atmos. Environ. 34 (10), 1553–1562.

Vaisala, 2021. Wind Energy WindCube. Vaisala. Available from: https://www.vaisala.com/en/wind-lidars/wind-energy/windcube. (Accessed 8 February 2021).

Wang, W., Ng, E., 2018. Air ventilation assessment under unstable atmospheric stratification—a comparative study for Hong Kong. Build. Environ. 130, 1–13.

Wang, W., Yang, T, Li, Y., Xu, Y., Chang, M., Wang, X., 2020. Identification of pedestrian-level ventilation corridors in downtown Beijing using large-eddy simulations. Build. Environ. 182, 107169.

Wang, W., Wang, X., Ng, E., 2021. The coupled effect of mechanical and thermal conditions on pedestrian-level ventilation in high-rise urban scenarios. Build. Environ. 191, 107586.

Wieringa, J., 1992. Updating the Davenport roughness classification. J. Wind Eng. Ind. Aerod. 41 (1–3), 357–368.

Wong, M.M.F., Fung, J.C.H., Ching, J., Yeung, P.P.S., Tse, J.W.P., Ren, C., Wang, R., Cai, M., 2019. Evaluation of uWRF performance and modeling guidance based on WUDAPT and NUDAPT UCP datasets for Hong Kong. Urban Clim. 28, 100460.

Xie, Z.-T., Castro, I.P., 2008. Efficient generation of inflow conditions for large eddy simulation of street-scale flows. Flow, Turbul. Combust. 81 (3), 449–470.

Xie, B., Fung, J.C., Chan, A., Lau, A., 2012. Evaluation of nonlocal and local planetary boundary layer schemes in the WRF model. J. Geophys. Res. Atmos. 117 (D12).

Yim, S.H.L., 2020. Development of a 3D real-time atmospheric monitoring system (3DREAMS) using Doppler LiDARs and applications for long-term analysis and hot-and-polluted episodes. Rem. Sens. 12 (6), 1036.

Yuan, C., Ng, E., 2012. Building porosity for better urban ventilation in high-density cities–A computational parametric study. Build. Environ. 50, 176–189.

Yuan, C., Adelia, A.S., Mei, S., He, W., Li, X.-X., Norford, L., 2020. Mitigating intensity of urban heat island by better understanding on urban morphology and anthropogenic heat dispersion. Build. Environ. 176, 106876.

Zealand, S.A.S.N., 2002. Australia/New Zealand Standard Structural Design Actions Part 2: Wind Actions, *AS/NZS 1170*, vol. 2, p. 2002.